



UNIVERSITY OF TRENTO - Italy

International Doctoral School in Biomolecular Sciences

XXV Cycle

**THE NEURONAL RNA BINDING PROTEIN HuB AS A  
POTENTIAL TUMOR SUPPRESSOR IN  
GLIOBLASTOMA**

Tutor : Dr **Alessandro Quattrone**

Advisor : Dr **Sara Leo**

Centre for Integrative Biology (CIBIO)

Laboratory of Translational Genomics

Ph.D. Thesis of

**Marta Tarter**

Centre for Integrative Biology (CIBIO)

Laboratory of Translational Genomics

Academic Year 2012-2013

## **ABBREVIATIONS AND ACRONYMS**

<b>Introduction</b>	
<b>GBM</b>	<i>Glioblastoma multiforme</i>
<b>EGFR</b>	<i>Epidermal growth factor receptor</i>
<b>PTEN</b>	<i>Phosphatase and tensin homolog</i>
<b>RB</b>	<i>Retinoblastoma 1</i>
<b>RTK</b>	<i>Receptor tyrosine kinases</i>
<b>EGF</b>	<i>Epidermal growth factor</i>
<b>PDGF</b>	<i>Platelet-derived growth factor</i>
<b>SVZ</b>	<i>Subventricular zone</i>
<b>SGZ</b>	<i>Subgranular layer</i>
<b>CSCs</b>	<i>Cancer stem cells</i>
<b>GSCs</b>	<i>Glioma cancer stem cells</i>
<b>NSCs</b>	<i>Normal stem cells</i>
<b>RBP</b>	<i>RNA binding protein</i>
<b>miRNA</b>	<i>microRNA</i>
<b>RRM</b>	<i>RNA recognition motif</i>
<b>ARE</b>	<i>AU-rich elements</i>
<b>3-5'UTR</b>	<i>3-5' untranslated region</i>
<b>IRES</b>	<i>Internal ribosome entry site</i>
<b>Materials and methods</b>	
<b>U-87 MG</b>	<i>Human glioblastoma cell line</i>
<b>H2b2T</b>	<i>Immortalized murine neuroepithelial cell line</i>
<b>GICs</b>	<i>Glioblastoma Initiating cells</i>
<b>FBS</b>	<i>Fetal Bovine Serum</i>
<b>EDTA</b>	<i>Ethylenediaminetetraacetic acid</i>
<b>LSI CDKN2A</b>	<i>Probe, labelled with Spectrum Orange, for CDKN2A locus</i>
<b>RP11-110I5</b>	<i>Probe, labelled with Spectrum Orange, for ELAVL2 locus</i>
<b>CEP 9</b>	<i>Probe, labelled with Spectrum Green for centromere</i>
<b>SDS</b>	<i>Sodium dodecyl sulfate</i>
<b>MECP2</b>	<i>Methyl CpG Binding Protein 2</i>

<b>ELAVL2</b>	<i>(Embryonic Lethal, Abnormal Vision, Drosophila)-Like 2 (Hu Antigen B)</i>
<b>CDKN2A /p16</b>	<i>Cyclin-Dependent Kinase Inhibitor 2A</i>
<b>CDKN1A /p21</b>	<i>Cyclin-Dependent Kinase Inhibitor 1A</i>
<b>INV1</b>	<i>Intervening region 1</i>
<b>INV2</b>	<i>Intervening region 2</i>
<b>CTDSP1</b>	<i>CTD (Carboxy-Terminal Domain, RNA Polymerase II, Polypeptide A) Small Phosphatase</i>
<b>SNRPF</b>	<i>Small nuclear ribonucleoprotein polypeptide F</i>
<b>B-TUB</b>	<i><math>\beta</math>-Tubulin</i>
<b>TBP</b>	<i>Tata Box Binding Protein</i>
<b>HPRT1</b>	<i>Hypoxanthine Phosphoribosyltransferase 1</i>
<b>B2M</b>	<i>Beta-2-Microglobulin</i>
<b>SOX2</b>	<i>SRY (Sex Determining Region Y)-Box 2</i>
<b>NES</b>	<i>Nestin</i>
<b>PFA</b>	<i>Paraformaldehyde</i>
<b>NaCl</b>	<i>Sodium chloride</i>
<b>HCl</b>	<i>Hydrochloric acid</i>
<b>MgCl</b>	<i>Magnesium chloride</i>
<b>p</b>	<i>p-value</i>
<b>DEGs</b>	<i>Differential Expression Genes</i>
<b>Result</b>	
<b>CNAs</b>	<i>Copy number alterations</i>
<b>qPCR</b>	<i>Quantitative real-time PCR</i>
<b>FDR</b>	<i>False discovery rate</i>

1. SUMMARY.....	6
2. INTRODUCTION.....	7
2.1 Glioblastoma.....	7
2.2 ELAVL proteins.....	10
2.3 HuB.....	14
2.4 ELAV in cancer.....	15
3. AIM OF THE THESIS.....	16
4. MATERIAL AND METHODS.....	17
4.1 CELLS CULTURE METHODS.....	17
4.1.1 General procedures.....	17
4.1.2 Generation of stable cell lines.....	17
4.1.3 Transient transfection.....	18
4.1.4 Scratch Assay.....	19
4.1.5 Cell Migration and Invasion Assay.....	20
4.1.6 Neurosphere assay.....	20
4.1.7 Fluorescent In Situ Hybridization (FISH).....	21
4.1.8 Fluorescence Activated Cell Sorting (FACS).....	21
4.2 MOLECULAR METHODS.....	22
4.2.1 RNA extraction and reverse transcription.....	22
4.2.2 Polysomal and sub-polysomal RNA extraction.....	22
4.2.3 Reverse transcription of polysomal and sub-polysomal RNA.....	23
4.2.4 Extraction of genomic DNA from paraffin samples.....	23
4.2.5 Quantitative PCR with SYBR green.....	24
4.2.6 qPCR with TaqMan probes.....	25
4.2.7 Microarray analysis.....	26
4.2.8 Luciferase assay.....	27
4.2.9 Plasmid construction.....	27
4.2.10-1 Generation of pGL4.13-p21-5'UTR-v1 and pGL4.13-p21-5'UTR-v2.....	28
4.2.10-2 Generation of pGL4.13-p21-3'UTR.....	29
4.2.11 qRT-PCR of H2b2T cells steadily expressing HuB.....	30
4.3 PROTEIN METHODS.....	31
4.3.1 Immunoblotting analysis.....	31
4.4 STATISTICAL ANALYSES.....	32
4.5 BIOINFORMATIC ANALYSIS OF GBM SAMPLES.....	32

5. <i>RESULTS</i> .....	34
5.1 Genome-wide analysis of RNA binding proteins expression alterations in GBM identifies HuB as a potential tumor suppressor protein. ....	34
5.2 HuB loss is a frequent event in GBMs.....	36
5.3 The patterns of codeletion of the CDKN2A and the ELAVL2 loci in GBM are suggestive of a modifier role of ELAVL2 loss in a CDKN2A loss background. ....	37
5.4 HuB modulation in U87MG cells and HuB reconstitution in glioma initiating cells indicate that HuB suppresses glioma cell migration and invasion. ....	39
5.5 Loss of HuB expression increases the degree of stemness in glioma cells. ....	42
5.6 HuB controls the expression of genes involved in cell adhesion and motility.....	44
5.7 The p21 tumor suppressor is translationally enhanced by HuB in mouse neural tube cells. .	46
6. <i>DISCUSSION</i> .....	48
7. <i>BIBLIOGRAPHY</i> .....	51
8. <i>APPENDIX</i> .....	62
Copy number alterations (CNAs) can be detected by qPCR using SYBR-GREEN .....	62

## **1. SUMMARY**

Post-transcriptional regulation is emerging as a fundamental step in gene expression that, when altered, can contribute to carcinogenesis. To identify potentially altered translational networks in glioblastoma multiforme (GBM), the worst of brain tumors, we correlated genomic alterations and mRNA levels of RNA-binding proteins (RBPs) in 372 publicly available GBM samples and identified 56 RBPs whose copy number alterations correlate with their altered expression levels in at least 15% of the samples. Among the genes identified using our parameters, HuB (ELAVL2) was deleted in 48% of the samples and down-regulated in more than 90% of these. Given the evidence for HuB activity as a differentiation factor in neuronal cells, we hypothesized that it may act as an oncosuppressor. However, ELAVL2 maps to the same chromosomal band (9p21.3) as CDKN2A, the most frequently inactivated oncosuppressor in gliomas, giving the possibility that ELAVL2 loss is simply a consequence to the CDKN2A deletion and therefore a passenger, albeit very frequent, mutation. To test this possibility, we analyzed the structure of the deletion spanning the two loci by qPCR analysis of 233 GBM samples, testing for the presence of the intervening region, and we obtained evidence that two independent focal deletions occurred in about 20% of the GBM samples bearing homo- and/or heterozygous deletion at CDKN2A and ELAVL2. This result highlights that, in rare but recurrent cases, ELAVL2 deletion occurs independently from CDKN2A deletion, supporting the hypothesis that loss of HuB activity is a condition contributing to tumor progression. This hypothesis was tested using U87MG cells, a commonly used glioma cell line homozygously deleted for CDKN2A and heterozygously deleted for ELAVL2 and primary glioma initiating cells (GICs) homozygously deleted for both genes. Migration, invasion and capacity to form neurospheres were determined in U87MG cells upon HuB silencing and overexpression, and in GICs upon HuB expression. HuB expression in both cell models resulted in a decreased in migration, invasivity and the capacity to form neurospheres, supporting the hypothesis that HuB act as a tumor suppressor. We finally showed that HuB is able to determine an increase of p21 protein in normal murine neuroblast cells, providing a possible mechanism for HuB-mediated suppression of glioma cell clonality.

## **2. INTRODUCTION**

### **2.1 Glioblastoma**

Glioblastoma multiforme (GBM) is the most frequent and aggressive type of glioma, a class of tumors arising from glia or their precursor in the human central nervous system. Also named glioblastoma by the World Health Organization (WHO), it is a IV grade of astrocytoma, a tumor associated with a dismal prognosis (1). The current standard of care for GBM is surgical resection followed by radiotherapy adjusted with the addition of temozolomide, an oral alkylating agent demonstrated to have an anti-tumoral activity in the treatment of recurrent glioma, with a statistically significant survival benefit and a minimal additional toxicity. Despite the use of this drug, the median survival is only 15 months ( 2, 3, 4 ). On the basis of clinical presentation, GBM has been categorized into two groups: “primary” and “secondary” (5). The majority of primary GBMs cases (90%) develop rapidly *de novo*, and at diagnosis appear as advanced cancers without clinical or histological history of a precursor lesion (5, 6). Tumors that have clinical, radiologic, or histopathologic evidence of malignant progression from a pre-existing lower grade tumor are considered secondary GBMs. Secondary GBMs occur less frequently (5% of GBMs) and predominantly in younger patients: the median age of these cancers is ~ 45 years versus ~ 60 years for primary GBMs. Despite these differences, secondary and primary GBMs are indistinguishable from a histopathologic point of view and the prognosis does not differ after adjustment for age (6, 7). Focusing on the identification of genetic alterations in GBMs helped to redefine differences between the two groups. Loss of 10q heterozygosity (70% of cases), *EGFR* amplification (36%), *p16<sup>INK4a</sup>* deletion (31%), and *PTEN* mutations (25%) are peculiar of primary GBMs. Whereas *TP53* mutations are the most frequent in the pathway of secondary GBMs. A recent study published by Parada et al. (8), confirmed previous data from Parson et al., indicating that the majority of GBMs have alterations in p53, RB and the RTK pathways (9, 10). Alterations in these three pathways fuel cell proliferation and enhance cell survival by dysregulating cell-cycle checkpoints, induction of senescence or apoptosis (*Figure 1*) .

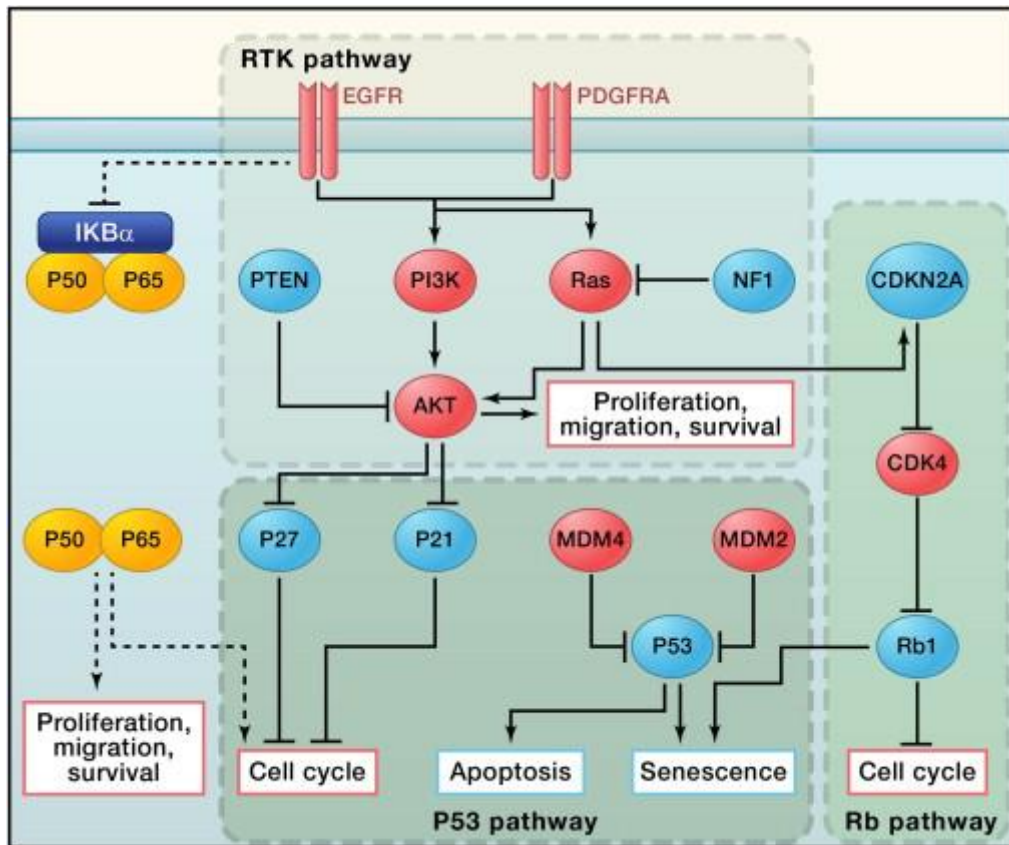


**Figure 1: Core signaling pathways in glioma tumorigenesis.** The receptor tyrosine kinase (RTK), p53, and Rb pathways are the core signaling pathways in glioma tumorigenesis. Red ovals indicate oncogenes that are either overexpressed or amplified in GBM samples, whereas blue ovals indicate tumor suppressor genes that are somatically mutated or deleted (except for p27 and p21). Source: Malignant Glioma: Lessons from Genomics, Mouse Models, and Stem Cells (8).

A widely accepted model for glioblastoma tumorigenesis assumes that this tumor arises from developmentally arrested progenitor cells localized in niches, such as the subventricular zone (SVZ) (111). Neural cells in the mouse SVZ include: a layer of ependymal type E ciliated cells facing the ventricle, relatively quiescent type B cells, which are responsive to growth factors such as EGF and PDGF, and give rise to transient amplifying type C cells, which in turn give rise to type A neuroblasts that contribute to the rostral migratory stream in most cases, forming olfactory bulb mature neurons (Figure 2. A). Cell proliferation in the niche is controlled by the RB1 signaling pathway (101). RB1 prevents E2F from promoting the G1/S transition, unless it is phosphorylated by the cyclin D-CDK4/6 and/or the cyclin E-CDK2 complexes. These two complexes are inhibited by the cyclin-dependent kinase inhibitor p16INK4A (encoded by CDKN2A, located on chromosome 9) and p21 WAF1/CIP1 (encoded by CDKN1A, on chromosome 6), respectively



(Figure 2 B). Although it is possible that type B, type A or even putative astrocyte precursor cells could give rise to glioblastoma, type C cells are predominantly implicated in the origin of this kind of tumor (56, 57, 58).

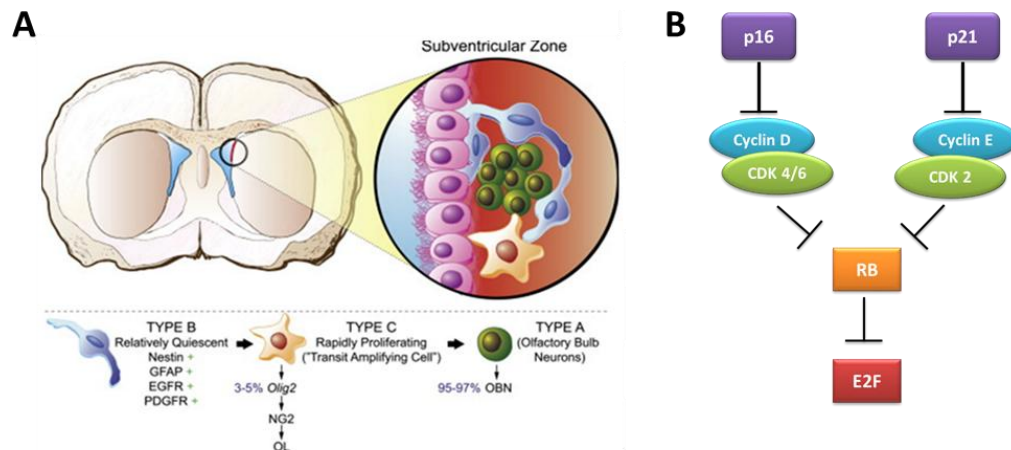


**Figure 2 : The subventricular zone (SVZ), the niche of germinal centres in the brain. (A)** Cells populating the SVZ. Neural Progenitor Subtypes in the Subventricular Zone (Top). Coronal section through the postnatal adult mouse forebrain depicts subventricular zone (SVZ) progenitors in situ including type B (blue), C (amber), and A (green) cells, as well as ciliated ependymal cells (pink) that line the lateral ventricle (see 56 for further reading). (Bottom) **(B)** RB pathway regulates cell proliferation in the niche. The two tumor suppressors p16 and p21 block the complexes cyclinD-CDK4/6 and cyclin-E/CDK2, respectively, which in turn prevents RB from blocking E2F. In this way E2F can induce the G1/S transition. Source: Glioma stem cells: a midterm exam (102)

A widely considered model for tumor formation hypothesizes the existence of cancer stem cells (CSCs), able to give rise to other types of malignant cells in the same way that normal stem cells do (11,12,13). CSCs are a sub-population in the tumor with self-renewal capacity which are able to generate all the heterogeneous cell types constituting the tumor (14). Glioma cancer stem cells (GSCs), isolated from human solid tumors(15, 16), share remarkable similarities with normal stem cells (NSC), expressing neural stem/progenitor cell markers, such as Nestin, Sox2 and Olig2. Moreover, GSCs can be differentiated *in vitro* to cells expressing neuronal or glial markers.

NSC resides in a specific region of the brain called niche, which is formed by the subventricular zone (SVZ) and the subgranular layer (SGZ) (17). In these regions, specific cells, such as ependymal cells and endothelial cells, cytoskeletal proteins and growth factors create a microenvironment providing support for the multi-potency and self-renewal of NSC. The same could be true for GSC (18). Germinal regions, such as SVZ, have been long suspected to be a possible source of gliomas (59, 60). Unsurprisingly, many gliomas are either periventricular or contiguous to the ventricular or sub-ventricular zone (61), and contain cells sharing phenotypic and behavioral characteristics with NSCs. Moreover, this subpopulation of cells within human

glioblastoma, exhibits a lower frequency of cell division, compared to the tumor cells, and also an enhanced ability to form tumors *in vivo*: features that are consistent with a tumor-initiating cell. They also possess the characteristic of long-term proliferation, self-renewal, generation of different progeny, and express the transmembrane glycoprotein prominin 1 (also known as CD133). As CD133 positive cells have been demonstrated to be efficient at initiating tumors, including human glioblastoma tumors, recent studies proposed to use CD133 as a marker for tumor initiating cells (19- 21).

## **2.2 ELAVL proteins**

For many years, gene regulation was believed to be controlled primarily at the transcription initiation level, the first step in the flow of information from genome to proteome (22). More recently however, comparisons between the transcriptome, translome and proteome indicate that gene regulation is largely dependent on complex networks of signals acting on mRNAs, which shape the proteome by changing mRNA accessibility to translation. Post-transcriptional regulation is controlled by an array of RNA binding proteins (RBPs) and non-coding RNAs and allow a rapid adjustment of the cell to environmental changes (23, 24).

Many proteins that regulate cell growth and differentiation are codified by unstable mRNAs, often characterized by cis-regulatory elements responsible for their degradation. One class of such elements is represented by the AU-rich elements (AREs) mainly present in 3' UTRs and bound by many RBPs, including members of the ELAVL family (25, 34).

The *embryonic lethal abnormal vision* (ELAV) gene, originally discovered in *Drosophila*, is essential for the development and maintenance of the nervous system (26, 62, 63). Vertebrates have four, highly-conserved (27-31), ELAV-like (ELAVL) proteins (also referred to as Hu proteins) belonging to the RNA-binding protein family of ARE-binding factor, a subfamily of the RNA recognition motif (RRM) superfamily. ELAVL1 (HuR/A) is expressed in all cell types and localizes primarily to the nucleus. Upon certain cellular signals (like stress signals) ELAVL1 shuttles to the cytoplasm, where it promotes translation of target mRNAs by mechanisms not entirely understood (35). The three other ELAVL proteins—ELAVL2 (HuB/HeI-N1), ELAVL3 (HuC), and ELAVL4 (HuD)—were discovered as auto-immune antigens in a neurological disorder termed paraneoplastic encephalomyelopathy (32) and are almost exclusively expressed in neurons (36). These three proteins are collectively referred to as neuronal ELAVL (nELAVL) proteins and localize predominantly to the cytoplasm, but they too have the ability to shuttle between nucleus and cytoplasm (33). ELAVL proteins have been involved in the regulation of all steps of RNA

metabolism, from pre-mRNA splicing to transport, stability and translation (64, 65) suggesting that they might act through different mechanisms.

The ELAVL proteins share both sequence and domain conservation. In mammals, the four members are 70-85% identical at the amino acid level. Structurally, they all contain three RRM, each of about 90 amino acids, and a variable hinge region. RRM1 and RRM2 are located one next to the other at the N-terminus, whereas RRM3 maps at the C-terminus and is separated from the other two by a highly variable hinge region (Fig. 3). RRM3 is able to bind the poly(A) sequence and to preserve the stability of RNA-protein complexes. Interestingly, the length of the poly(A) tail seems to correlate with efficiency of the binding of ELAVLs to their mRNA targets. For instance, HuD has a ~10 fold higher binding affinity for its target GAP-43 long tail versus short tail (66). RRM1 and RRM2 are instead important for binding to ARE sequences present in target RNAs (37-41). The hinge region, which varies between the different members of the family, seems to be necessary for shuttling the proteins between nucleus and cytoplasm. For example, in the hinge region of HuR are present both a nuclear localization signal and a nuclear export signal (67).

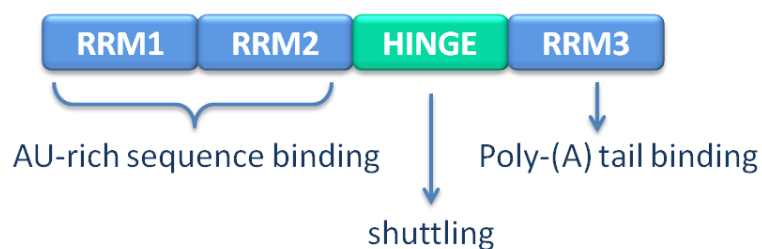


**Figure 3: ELAVL protein domains and their function.** Not in scale.

ELAVL proteins preferentially bind AU-rich elements (AREs) sequences, although they share a high affinity also for other consensus sequences endowed with U-rich, C-rich and GU-rich nucleotides (42-45). About 5-8% of human genes contains AREs, usually located in 3'UTRs, but also in 5'UTRs and/or in coding sequences (46), acting as instability elements (47). In most cases, ELAVL binding to these regions increase the expression of the target mRNA (48). Recent studies found that ELAVL proteins can also bind ARE or U/GU-rich sequences belonging to intronic regions (43-45), suggesting a possible involvement of these proteins in splicing events. In many instances, binding of ELAVL proteins to their target mRNAs, do not affect mRNA turnover, but promote the recruitment of the target mRNA to polysomes, which leads to an increase in their translation. For example, HuR enhances the translation of cytochrome c and p53, and HuB increases the translation of neurofilament M (68-70), without changing the levels of the corresponding mRNAs. In some cases, ELAVL proteins can also act by stabilizing the target

mRNAs in addition to promoting the recruitment to polysomes. For example, HuB binds and stabilizes the glucose transporter (GLUT1) mRNA, but also promote the formation of translation initiation complexes (71). Finally, ELAVL proteins may act as repressors of translation on some targets. This is the case for HuR and HuD that suppress p27 translation by inhibiting IRES-mediated initiation (72).

A partial list mRNA targets for ELAVL proteins is reported in Table 1, indicating the activity exhibited for each targets. The identities of the mRNA targets for the nELAVL proteins highlight their roles in the neuronal differentiation program: transcription factors active in neuronal lineage (c-fos, c-myc, N-myc, Id), microtubule markers for neuronal development (tau, neurofilament M), determinants of neurite outgrowth and synapse formation (GAP-43, neuroserpin) and regulators of neuronal proliferation/differentiation (p21, p27, musashi 1). Several experimental findings demonstrated that nELAVL proteins are necessary and sufficient to induce neuronal differentiation *in vitro* models and to trigger neuronal commitment in neural stem/progenitor cells (49, 54).

**Table 1: Known nELAVL target mRNAs.** Source: *Defining a neuron: neuronal ELAV proteins (25).*

<b>Protein</b>	<b>Target mRNAs</b>	<b>Activity</b>	
<b>HuB</b>	c-myc <sup>103</sup>		
	c-fos <sup>103</sup>		
	GM-CSF <sup>103</sup>		
	GLUT1 <sup>104</sup>	Increased stability and translation	
	NF-M	Increased translation	
	Id <sup>105</sup>		
<b>HuC</b>	c-myc <sup>106</sup>		
	VEGF <sup>106</sup>		
<b>HuD</b>	c-myc <sup>106,107</sup>		
	N-myc	Increased stability and expression	
	c-fos <sup>39</sup>		
	VEGF <sup>106</sup>		
	p21 <sup>108</sup>	Increased stability and expression	
	p27	Inhibition of translation	
	acetylcholinesterase <sup>109</sup>	Increased stability	
	GAP-43 <sup>110</sup>	Increased stability	
	tau	Increased stability	
	neurosperrin <sup>111</sup>	Increased expression	
	musashi-1 <sup>112</sup>	Increased stability	
	MARCKS <sup>113</sup>	Increased stability	
	CGRP/calcitonin <sup>114</sup>	Regulation of alternative splicing	
	<b>HuR</b>	cytrocromo c <sup>69</sup>	Increased stability
		p53 <sup>68</sup>	Increased stability
p27 <sup>71</sup>		Inhibition of translation	
p21 <sup>65</sup>		Increased stability	
cyclin D <sup>65</sup>		Increased stability	

### 2.3 HuB

Human *elav*-like neuronal protein 1 (Hel-N1, also known as ELAVL2 or HuB) was cloned by the Keene's laboratory, screening a human fetal brain library with a conserved sequence spanning RRM 1 and 2 of the *Drosophila elav* gene as a probe (34). The gene was mapped to chromosome 9p21 (124), close (~2 megabases) to the locus of p16 (CDKN2A), a tumor suppressor often deleted in many type of cancers (8). Three transcript variants encoding for two different isoforms have been identified (Figure 4).

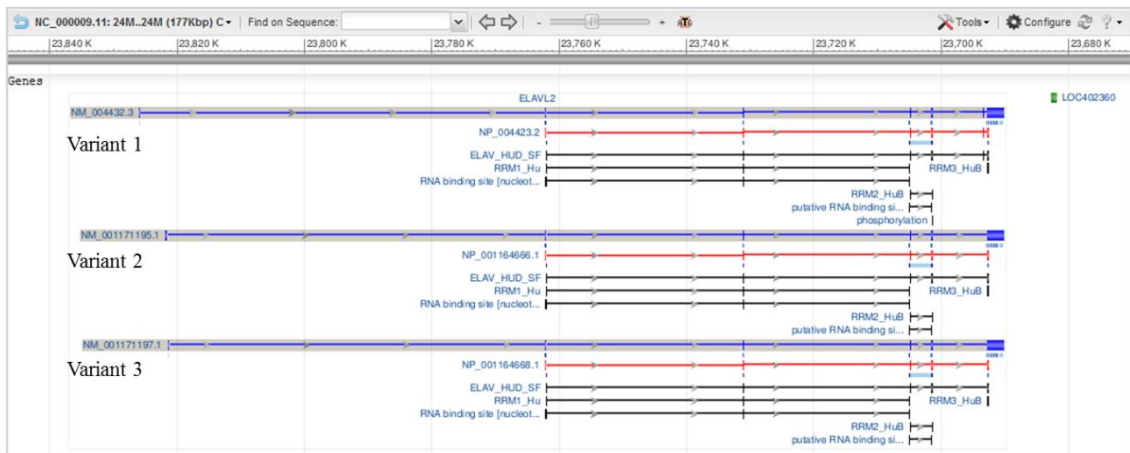


**Figure 4: Transcript variants for the human ELVL2 gene.** Vertical bars represent exons. Red line represents the protein (not in scale). Location of each RRM is reported. Comparison with HuD (ELAV\_HuD\_SF) is shown as a reference, as it is the best characterized member of the nELAVL proteins (76).

Transcript variant 1 encodes for the longest isoform (Hel-N1 or isoform a; 359 amino acids), whereas transcript variants 2 and 3 differ in the 5'UTR and lack an alternate in frame exon compared to variant 1. The resulting isoform (Hel-N2 or isoform b; 346 amino acids) has the same N- and C-termini, but lack 13 amino acid residues between RRM2 and 3, compared to isoform a. Hel-N2 is expressed in several cultured cellular lines, including neuronal precursors, but is absent in mature neurons (REF).

Both isoforms shares ~80% sequence identity with the other members of the ELAVL family (25). The protein is well conserved within vertebrates (27-31). The mouse have four ELAVL2 isoforms, which share 96 to 99% identify at the amino acid level to the human isoforms. Chicken have three ELAVL2 isoforms, which are 96% identical to Hel-N1.

*In vitro* RNA binding experiments demonstrated the ability of HuB to bind 3'UTRs of *c-myc*, *c-fos*, colony-stimulating factor and the Id transcriptional repressor, which is abundantly expressed in

undifferentiated neural precursors (34, 64). The protein expression was found to be restricted to the nervous system and, unlike HuC and HuD, gonads (34, 27, 64, 73). The subcellular localization is mainly cytoplasmic, where the protein is detected in granular particles in the soma and along the proximal regions of dendrites (64).

ELAVL2 is an early marker of neuronal commitment. *In situ* hybridization experiments performed on murine embryos show that HuB is the first nELAVL protein to be expressed, in very early post-mitotic neurons of the ventricular zone, in the intermediate zone and diminishing in the cortical plate, whereas in adult mice it is detectable only in scattered neurons (36, 74).

Overexpression of HuB in several cell lines induces neuronal differentiation (26, 51, 55) and ectopic transfection of HuB into human teratocarcinoma NT2 cells induces formation of neurites (51). Ectopic misexpression of HuB in the mouse neural tube determines the presence of neuronal markers (55).

ELAVL2 binding to transcription factors involved in neuronal differentiations (*c-fos* and *c-myc*) and microtubules markers of neuronal development (NF-M; Table 1) suggest an important role in neuronal development.

Experiments with murine neuroblastoma cells show that HuB, as well as HuR and HuD, up-regulate p21 mRNA expression. The silencing of p21, decreases HuB activity, suggesting that p21 is its downstream effector for differentiation induction (49).

#### **2.4 ELAV in cancer**

Of all ELAVL proteins, the role of HuR in cancer development has been most extensively studied. HuR is associated with poor survival in esophageal cancer (75) and has been involved in sarcoma development, binding and degrading the tumor suppressor A20 (76). Moreover, HuR expression is found in pancreatic, colon and liver cancer as well as in oral squamous carcinoma cells (77-80). Recent studies suggest that anti-HuC and -HuD auto-antibodies are novel differential sero-diagnostic markers for small cell lung carcinoma (SCLC) (81) and large cell neuroendocrine carcinoma (LCNEC) (82). Results on SCLC and carcinoid tissues support the hypothesis that alterations of nELAV genes could be involved in the onset and/or progression of a subset of neuroendocrine lung tumors (83).

### **3. AIM OF THE THESIS**

To investigate the molecular mechanisms leading to glioblastoma multiforme (GBM), the most frequent and aggressive class of tumors arising from glia or their precursors in the human central nervous system, we started by correlating copy number alterations commonly found in GBM and changes in the expression levels of the correspondent RNA-binding proteins (RBPs). Data mining of publicly available resources (TCGA Consortium, 2008) identified 56 RBPs, whose expression levels are significantly altered in GBM. Among these, we focused on HuB (ELAVL2/HeI-N1), deleted in 48% of the sample and down-regulated in more than 90% of these, because it belongs to a class of RBPs directly involved in neuronal development.

The ELAVL2 gene maps on chromosome 9p21, close (~2 megabases) to the p16 (CDKN2A) gene, which codes for a cyclin-dependent kinase inhibitor often deleted in GBM as well as in many other cancers (86,101). Considering the relevance of p16 mutations in oncogenesis, we tested whether the deletion of the nearby ELAVL2 gene was the result of an expansion of the p16 deletion or the two mutations arose independently. To this aim, we analysed the region spanning the two genes by quantitative PCR (qPCR) using genomic DNAs from a collection of 233 GBM samples collected at the Verona Borgotrento hospital (Verona, Italy). Testing the presence of the intervening region between the two loci in samples bearing deletions of both ELAVL2 and CDKN2A genes, we found an intact intervening region in about 20% of the cases, proving that, in a minority of GBM samples, deletion of ELAVL2 is a secondary and independent event from CDKN2A deletion. From these results and the fact that HuB is involved in neuronal development, we hypothesized that ELAVL2 may act as an oncosuppressor, suggesting that its loss might be a required mechanism for tumor progression. To test this hypothesis, two GBM cell models, U87 MG cells and primary glioma initiating cells (GICs), both lacking CDKN2A, were used. In U87 cells, which are heterozygously deleted for ELAVL2, HuB expression was down-regulated or over-expressed, whereas in GICs, which are homozygously deleted for ELAVL2, HuB was over-expressed. In these two cell models, changes in migration, invasion and capacity to form neurospheres under different levels of HuB were determined.

Finally, it was tested the involvement of HuB in the regulation of p21 in non-tumorigenic, immortalized neuroepithelial cells. To this aim, murine HuB (mHuB) overexpression was induced in H2b2T cells, which were used as a convenient neuronal progenitor model, and the steady-state levels of p21 mRNA and protein were determined. Since we noticed a significant upregulation of p21 protein upon HuB overexpression we tested which part of the mRNA for p21 was important to mediate this activity.



## **4. MATERIAL AND METHODS**

### **4.1 CELLS CULTURE METHODS**

#### *4.1.1 General procedures*

All cell lines were grown in flasks (Corning, 430641) at 37°C, 5% CO<sub>2</sub> and 95% humidity.

U-87 MG, a human glioblastoma cell line, were cultured in Dulbecco's modified Eagle medium (DMEM high glucose; Gibco, 10938-025) supplemented with 10% Fetal Bovin Serum (Lonza, DE14-801 F) and 5x10<sup>4</sup>U Penicillin/Streptomycin (Lonza, DE17-602 E).

U-87 were cultured as neurospheres with Neurobasal® Medim (Invitrogen, 21103-049) supplemented with 20 nM of hrFGF (Sigma, F 0291), 20nM of EGF (Sigma, E 9644) and 10nM of LIF (Sigma, L 5283) for 6 days (85).

H2b2T, an immortalized murine cell line, was cultured in RPMI 1640 Medium GlutaMAX (Invitrogen, 61870-010), supplemented with 5 x 10<sup>4</sup>U Penicillin/Streptomycin (Lonza, DE17-602E) and 10% Fetal Bovine Serum (Lonza, DE14-801F).

Human glioblastoma initiating cells (GICs# 030616) were derived from human brain after a dissection procedure described in reference (84), and were kindly provided by Dr. Rossella Galli (Fondazione San Raffaele Del Monte Tabor, Milan). They were cultured as neurospheres with Neurobasal Medium (NeuroCult™ NS-A Proliferation Kit; Stemcell, 05750), supplemented with EGF (R&D System, 236-FB), FGF (R&D System, 233-FB) and Heparin (Sigma, H3393) following the protocol described in reference 84.

#### *4.1.2 Generation of stable cell lines*

All stable cell lines were created following the Lamia Lab Viral Production and Infection Protocol (tronolab.epfl.ch/lentivectors). Briefly, HEK-293T cells were transfected with 10 µg of ΔR (a plasmid coding for the virion packaging system), 5µg of VSVG (a plasmid coding for the virion envelope) and 20 µg of the plasmid of interest. 48 hours post infection the supernatant from the cell culture was collected and, together with reverse transcriptase (0.8 U/ml), were added to the cells of interest.

U87 stable lines (indicated as U87 sh-HuB in all figures), were created using an shRNA lentiviral vector to silence ELAVL2 (GIPZ Human ELAVL2 shRNA; Thermo Scientific, Clone ID:

V3LHS\_639120) and pCMV6-AN-GFP (Origene, PS100019) for the control line (U87 sh-CTR in all figures). The cells were selectively maintained using 50ug/μl of puromycin (Sigma, P8833).

To generate H2b2T cells stably over-expressing ELAVL2 (indicated as H2b2t st-HuB in all figures), HuB\_CMVpLenti Dest PURO was used: this vector contains the cDNA of murine ELAVL2 (NM\_207685.1) transcript variant 2. As a control (H2b2T st-CTR in all figures), CMVpLenti Dest PURO (Addgene, 17452) empty plasmid was used. The cells were selectively maintained using 100ng/μl of puromycin (Sigma, P8833).

Stable over-expression of ELAVL2 in GICs (indicated as GICs-HuB in all figures) was created using pLenti CMV GFP DEST (736-1) (Addgene, 19732), containing the cDNA of human ELAVL2 transcript variant 2 (NM\_001171195.1); the control (GICs-CTR in all figures) was obtained with an LR-CLONASE between pENTR-DsRed2 N1 (Addgene, 22523) and pLenti CMV Puro DEST (Addgene, 17452).

#### 4.1.3 Transient transfection

To achieve transient over-expression of ELAVL2, U87 MG cells were transfected with a mammalian expression vector for ELAVL2 (indicated as U87-HuB in all figures) or a control vector (U87-CTR in all figures). The plasmid used for ELAVL2 over-expression was pCMV6-Neo (Origene, pCMV6NEO), containing the cDNA of human ELAVL2 transcript variant 2 (NM\_001171195.1). For generating the control cells, the empty pCMV6-Neo (Origene, pCMV6NEO) plasmid was used. Cells were seeded in six-well plates (Corning, 3516), at a density of  $3 \times 10^5$  cells/well or in 100 mm plates (Corning 430167), at a density of  $6 \times 10^6$  cells/plate. After 24 hours the medium was replaced with Opti-MEM medium (Life Technology, 11058-021) and the cells were transfected. For transfection, two separate solutions were prepared: (a) 10 μl of lipofectamine (Invitrogen, 11668-019), mixed with 240 μl of medium, and (b) 4 μg of plasmid DNA diluted in ~250 μl of medium. Both solutions were left at room temperature for 5 minutes, then mixed together and incubated at room temperature for 20 minutes. The final 500μl mixture was added to the medium of each well. 4-5 hours post-transfection the cells were visually inspected and if the viable cells were at least at 80%, the Opti-MEM was replaced with DMEM.

In the same way H2b2T cells were transfected with a mammalian expression vector for HuB (pCMV6-Entry-HuB) or a control vector (pCMV6-Neo-empty). The cells were sown in a six-well plates (Corning, 3516),  $1,5 \times 10^5$  for well, or in petri plates (Corning 430167),  $6 \times 10^6$  for plate. 24 hours later the medium was replaced with of Opti-MEM medium (Life Tecnology, 11058-021)

and the cells were transfected. The plasmid used for HuB over-expression (indicated as H2b2t-HuB in all figures) was Elavl2 (NM\_207685.1) Mouse cDNA ORF Clone (Origene, MR219803): “Myc-DDK-tagged ORF clone of *Mus musculus* ELAV (embryonic lethal, abnormal vision, *Drosophila*)-like 2 (Hu antigen B) (ELAVL2), transcript variant 1 as transfection-ready DNA”. For control cells (indicated as H2b2t-CTR in all figures) the empty pCMV6-Neo (Origene, PCMV6NEO) plasmid was used. 4-5 hours post-transfection the cells were visually inspected and, if the viable cells were at least at 80%, the Opti-MEM was replaced with RPMI 1640.

Table 2 below shows the name used for each type of cell in the different experiments.

**Table 2: Acronyms used for each type of cell in the different experiments.**

<i>Cells type</i>	<i>Name</i>	<i>Feature</i>	
<b>U-87</b>	U87 sh-scr	<i>scramble</i>	<i>Stable transfection</i>
	U87 sh-HuB	<i>Elavl2 knock-down</i>	<i>Stable transfection</i>
	U87-CTR	mock	<i>Transient transfection</i>
	U87-HuB	Elavl2 over-expression	<i>Transient transfection</i>
<b>GICs</b>	GICs-CTR	scramble	<i>Stable transfection</i>
	GICs-HuB	Elavl2 over-expression	<i>Stable transfection</i>
<b>H2b2T</b>	H2b2t st-CTR	scramble	<i>Stable transfection</i>
	H2b2t st-HuB	Elavl2 over-expression	<i>Stable transfection</i>
	H2b2t-CTR	mock	<i>Transient transfection</i>
	H2b2t-HuB	Elavl2 over-expression	<i>Transient transfection</i>

#### 4.1.4 Scratch Assay

U87-shHuB cells and U87-shCTR cells were seeded –  $5,0 \times 10^5$  per well – in a transparent 6-well plate (Costar, 3516), in 2 ml of DMEM (*see paragraph 3.1.1*) medium. After 24 hours of incubation at 37°C, time sufficient to reach confluence, the cells were scraped with a P200 pipet tip in a straight line to create a “scratch”. The images were acquired every 60 minutes over the course of 7 hours. The test was performed with 6 technical replicates per condition, in 3 different biological replicates.

#### 4.1.5 Cell Migration and Invasion Assay

Adherent cells were incubated for 24h at 37°C, time sufficient for them to reach confluence, after which they starved for 8 hours, by means of growing them without FBS. At the end of the starvation period, cells were seeded into migration/invasion upper chambers (Millipore, ECM509 and ECM554 ) in medium without serum. As chemoattractant, in the lower chamber, the medium was supplemented with 2% of serum. The size of membrane's pores were 8 µm. The assay was performed using three biological replicates, each of them consisting of three technical replicates.

U87-shHuB cells and U87-shCTR cells were sown –  $5,0 \times 10^5$  per well – in a transparent 6-well plate (Costar, 3516), in 2 ml of DMEM complete medium (*see paragraph 3.1.1*). After 8 hours of starvation,  $3,0 \times 10^5$  cells were sown in each upper chamber containing 250µl of DMEM without serum and, in the lower chamber, 500 µl of DMEM with 2% of serum was supplied. The same protocol was used for the transiently transfected cells, U87-HuB and U87-CTR.

H2b2T-stHuB cells and H2b2T-stCTR cells were sown –  $3,5 \times 10^5$  per well – in a transparent 6-well plate (Costar, 3516), in 2 ml of RPMI complete medium (*see paragraph 3.1.1*). Therefore, after 8 hours of starvation,  $3,0 \times 10^5$  cells were sown in each chamber containing 250µl of RPMI without serum and, in the lower chamber 500 µl of RPMI with 2% of serum as chemoattractant.

GICs-HuB cells and GICs-CTR cells were sown –  $2.5 \times 10^5$  per well – in a transparent 6-well plate (Costar, 3516), in 2 ml of Neurobasal complete medium (*see paragraph 3.1.1*). After an incubation of 5 days at 37°C, time required for neurospheres formation, the neurospheres were centrifuged at 1000 x g for 10 minutes and the pellet was re-suspended in 1ml of PBS (Gibco, 10010-015). Cell dissociation was achieved by the addition of 1/20<sup>th</sup> of the resuspension volume of a 1:1 solution of Trypsin (Gibco, R-001-100) and PBS supplemented with 2mM of EDTA (Sigma, E6758), followed by repeating pipetting up and down to disaggregate the neurospheres. This cell suspension was loaded into the upper chamber and the complete neurobasal medium (*see paragraph 3.1.1*) was used as a chemoattractant in the lower chamber.

#### 4.1.6 Neurosphere assay

U-87 cells were cultured as neurospheres in 96-well plates (Costar, 3595) for six days. For each conditions 10 wells containing 200µl medium with 20 cells/µl were prepared, and only spheres that exceeded 100 µm in diameter were considered as neurospheres. Images were captured using an

inverted microscope LEICA DM IL LED and analysed using Leica LAS EZ software (version 1.5.0, Leica Application Suite).

GICs derived from the dissociation of neurospheres were seeded in 96-well plate (Costar, 3595), 20 cells/ $\mu$ l in 200 $\mu$ l were sown in each well (87). Images were acquired using Operetta PerkiElmer High content Screening System with a 2X long WD objective, which allows to image an entire well. GICs-RED were imaged with 520-550 nm Ex filter and 560-630 nm Em filter, and GICs-GFP with 460-490 nm Ex filter and 500-580 nm Em filter. For each condition 10 wells were analyzed automatically by Harmony Software. The first step of the image analysis sequence was the identification of spheres. After removal of objects touching the border of the well, they were further analyzed by measuring their morphology properties. Finally the population of spheres having a diameter greater than 100  $\mu$ m and a roundness greater than 0.8 were selected and counted.

#### 4.1.7 Fluorescent In Situ Hybridization (FISH)

Paraffin GBM samples, kindly provided by Dr. Andrea Talacchi and Dr. Claudio Ghimenton (BorgoTrento Hospital, Verona, Italy) were prepared in triplicates on slides using Manual Arrayer (Beecher Instruments, Micro-Array Technology), and the size of the core was of 1mm in diameter. Vysis LSI CDKN2A/CEP 9 Probes Kit was used to identify the presence of CDKN2A. LSI CDKN2A (p16) probe was labelled with SpectrumOrange and the CEP 9 probe was labeled with SpectrumGreen. The LSI CDKN2A probe spans approximately 222 kb and contains a number of genetic loci including D9S1749, DS1747, p16 (INK4B), p14 (ARF), D9S1748, p15(INK4B), and D9S1752. The CEP 9 SpectrumGreen probe, hybridizing to alpha satellite sequences specific to the centromere of chromosome 9, was used as control for chromosome 9. The presence of ELAVL2 was analyzed using BAC RP11-110I5 (which covers the entire ELAVL2 locus) labeled with SpectrumOrange. Nuclei were stained with Dapi (Sigma, D 9542). The analysis was performed in blind by 2 groups using Zeiss Axio Observer Z1- Apotome.

#### 4.1.8 Fluorescence Activated Cell Sorting (FACS)

GICs cells overexpressing ELAVL2 (GICs-HuB) and control cells (GICs-CTR) were sorted using a FACSAria cytometer (DB Biosciences, San Diego, CA). The emission filters used were BP 530/30 for GICs-GFP (FITC) and BP 585/42 for GICs-Red (PE). Between each fluorescence spectrum, appropriate values of electronic compensation were adjusted. Debris and duplets were excluded from the analysis. Dissociated cells were resuspended in PBS (Gibco, 10010-015), 2mM EDTA

and 1% of Penicillin/Streptomycin. Cell suspension was passed through a 30µm filter (Filcons, 130-33s) and analysed using the FACSAria cytometer. Cell populations were isolated, at room temperature, in polystyrene tubes (BD Biosciences, 352054) using a 100µm nozzle aperture, 20 psi pressure, with an average of 2000 events/sec. Data were analyzed with FACSDiva data analysis software (BD Biosciences), which gave a purity of 96.5% for GICs-Red and 97% for GICs-GFP.

The CycleTEST PLUS DNA Reagent Kit (BD Biosciences, 340242) was used to analyze the cell cycle of GICs cells. About  $5 \times 10^5$  of cells were used for analysis following the manufacturer's instructions. Briefly, the test was performed after seven days of culture in neurosphere condition. The emission filters used were LP 670 for PI (PercP), BP 530/30 for GICs-GFP (FITC) and BP 585/42 for GICs-Red (PE).

## **4.2 MOLECULAR METHODS**

### 4.2.1 RNA extraction and reverse transcription

Total RNA was extracted using RNeasy Plus Mini Kit (Qiagen, 73404), which allows for elimination of DNA, and quantified using a spectrophotometer (Nanodrop N1000). Reverse transcription was performed with 200ng of total RNA using iScript cDNA Synthesis Kit (Biorad, 170-8890), following the manufacturer's instructions.

### 4.2.2 Polysomal and sub-polysomal RNA extraction

Cells were grown in 100 mm dishes (Corning, 430167) until they reached ~80% confluency. Polysomes were stalled by incubating the cells with 10 µg/ml of cyclohexamide (Calbiochem, 239763) at 37°C for 3-4 minutes. After two washes with 5 ml of ice-cold PBS (Gibco, 10010-015) supplemented with 10 µg/ml of cyclohexamide, the cells were treated with 300 µl of ice-cold Lysis Buffer (10 mM NaCl, 10 mM MgCl<sub>2</sub>, 10 mM Tris-HCl pH 7.5, 1% Triton-X 100, 1% sodium deoxycholate, 0.2 U/µL RiboLock RNase inhibitor, 1 mM dithiothreitol, 0.01 mg/ml cycloheximide), scraped with a cell scraper (Sarsted, 83.1832), transferred to a pre-chilled 1.5 ml microcentrifuge tube and centrifuged at 16000 x g for 5 minutes at 4 °C to pellet the nuclei.

After preparation of sucrose gradients and centrifugation of the samples at 197 000 x g in a Sorval WX Ultracentrifuge for 1 h 40 min at 4°C, the gradient was fractionated using a Teledyne Isco model 160 gradient analyser, equipped with a UA-6 UV/VIS detector, collecting 1 ml fractions.

#### 4.2.3 Reverse transcription of polysomal and sub-polysomal RNA

Each polysomal fraction was digested at 37°C for 1-2 hours with 100 µg/ml proteinase K (Qiagen, 19131) and 1% SDS (Sigma, L3771). 250 µl of phenol/chloroform/isoamyl alcohol (Sigma, P2069) was added to each sample, mixed well and centrifuged at 16 000 x g for 5 minutes at 4°C. Subsequently, the upper, aqueous phase was transferred to a fresh tube, 1 ml of isopropanol (Sigma, I9516) was added and the samples were placed at -80°C for 1-2 hours. After a centrifugation at 16 000 x g for 30-40 minutes, the supernatant was removed and the pellet was subjected to purification using RNeasy Plus Mini Kit (Qiagen, 73404).

#### 4.2.4 Extraction of genomic DNA from paraffin samples

Genomic DNA was extracted from 233 paraffin tissue samples (diagnosed in the 2006-2009 period) of glioblastoma multiforme (GBM), kindly provided by Dr. Andrea Talacchi and Dr. Claudio Ghimenton (BorgoTrento Hospital, Verona, Italy) and analysed for copy number variation (CNV). Samples were first subjected to deparaffination and then the genomic DNA was extracted.

To remove the paraffin, 1 ml of Xilene (Sigma, 396052) was added to each sample (composed of 4-6 slides), vortexed for 10 minutes and centrifuged at 16 000 x g for 5 minutes. The supernatant was discarded and the procedure was repeated. 1 ml of absolute ethanol (Sigma, 02860) was added to each pellet, vortexed for 10 minutes and centrifuged at 16 000 x g for 5 minutes. The supernatant was discarded and the ethanol wash repeated once more. After removing the ethanol, 360 µl of buffer ATL (Qiagen, 19076) and 40 µl of proteinase K (Qiagen, 19131) were added to the pellets, and an overnight incubation in a thermomixer (Eppendorf, thermomixer comfort) at 55°C and 450 rpm was performed.

After cooling down the samples, 8 µl of RNase A (Qiagen, 19101) were added, samples were incubated at room temperature for 2 minutes and centrifuged for 30 seconds at 6000x g. 200 µl of buffer AL (Qiagen, 19075) were added to the samples and an incubation in thermomixer was performed at 70 °C for 10 minutes. The samples were then centrifuged for 30 seconds at 6000 x g. 200µl of absolute ethanol (Sigma, 02860) were added and the samples were centrifuged for 30 seconds at 6000 x g. The supernatant was transferred to a DNeasy spin column (Qiagen, 1011707) and centrifuged for 1 minute at 6000 x g. The flow-through was discarded, 500µl of buffer AW1 (Qiagen, 19081) were added to the column and a centrifugation at 6000 x g for 1 minute was performed. The flow-through was discarded, 500µl of 80% ethanol were added to the column and a centrifugation at 20 000 x g for 3 minute was performed. The column was left for 1 minute at room temperature in a new tube with 100 µl of nuclease free water (Qiagen, 129114), then it was

centrifuged at 6000 x g for 1 minute and the amount of gDNA was quantified using a spectrophotometer (Nanodrop N1000).

#### 4.2.5 Quantitative PCR with SYBR green

Primer Plus (<http://www.bioinformatics.nl/cgi-bin/primer3plus/primer3plus.cgi>) was used to design primers for target genes MECP2, CDKN2A, and ELAVL2, two intervening regions between the last two genes (INV1 and INV2) and for two reference genes: SNRPF and CTDSP1. Subsequently, a BLAST search (<http://blast.ncbi.nlm.nih.gov>) was performed to evaluate the specificity of these primers which were synthesized by Eurofins MVG Operon. Triplicate wells of simplex (CDKN2A, ELAVL2, INV1 and INV2, SNRPF and CTDSP1) reactions containing a series of 10-fold dilutions of DNA samples (100-0.01 ng/reaction) were used to determine the PCR efficiency of each primer pair, assessed by performing a melting curve analysis of the PCR template. qPCR reactions were carried out in triplicate on 384-well reaction plates (Bio-Rad, HSP 3805) with KAPA SYBR FAST qPCR MAster Mix (RESNOVA, KK4601), using CFX384 Real-Time PCR Detection System (Bio-Rad, 185-5384). The qPCR reaction was performed with 15ng of gDNA. *Table 3* lists the sequences of the oligonucleotides used for this analysis.



**Table 3: Primers used in qPCR to detect CNAs on genomic DNA of GBM samples.**

<i>Primer name</i>	<i>Accession</i>	<i>Position</i>	<i>Sequence</i>	<i>Amplicon size</i>	<i>Primer concentration [FINAL]</i>
<i>MECP2</i> f r	NT_167198.1	chrX: 4,215,430- 4,215,347	GAGTGGGAAGTTCTCAAGGTAGCA TGCTTCCGCAGCTATTCCA	84	200nM 200nM
<i>CDKN2A</i> f r	NT_008413.18	chr9: 21,958,172- 21,958,276	CTTCGGTGACTGATGATCTAAGTTTC GTTTCTAACGCCTGTTTCTTTCTG	105	400nM 400nM
<i>ELAVL2</i> f r	NT_008413.18	chr9: 23,725,162- 23,725,243	AAAAATTTGCCTGGTAACTGAACAT TGACCACAGGTAGCTTCTGAGAAT	82	400nM 400nM
<i>INVI</i> f r	NT_008413.18	chr9: 22,742,705- 22,742,798	TGGAGGCAGAGCTGAGGAAT GAAGGCTCAAGATTTTGTTCATC	94	400nM 400nM
<i>INV2</i> f r	NT_008413.18	chr9: 23,428,171- 23,428,275	CTATAAGCAAGGAGCCAAGATATGC GGTTGGAGTAGAACCCCACTGA	105	400nM 400nM
<i>SNRPF</i> f r	NT_029419.12	chr12: 58,396,439- 58,396,542	AGAATTTGCACTTCCCCTTAACC TGTCTCCCCACCCAAGTGA	104	400nM 400nM
<i>CTDSP</i> f r	NT_005403.17	chr2: 69,476,893- 69,477,005	CCCCTGGATTCTGCACTAG CCGCCAGAAAACGATCAAAAC	113	400nM 400nM

Oligonucleotides were synthesized by Eurofins MVG (<http://www.eurofinsgenomics.eu/>). Amplifications were performed over 40 cycles, including a denaturation (95°C, 15 seconds), an annealing step (60, 20 seconds) and an extension step (72°C, 1 minute). Each reaction was performed including an internal control consisting of the gDNA from the same pool of samples, but with a normal copy number of the region studied. The results were obtained using the  $2^{-\Delta\Delta Ct}$  method. Data acquisition and the analysis of the qPCR assays were performed using CFX Manager™ Software 184-5000 (Version 3.0, Bio-Rad).

#### 4.2.6 qPCR with TaqMan probes

Analysis of stemness (SOX2 and NESTIN,) of p21 and ELAVL2 genes were performed using Taqman probes. Probes were supplied by Life Technologies (<http://www.invitrogen.com>). The probes used for these validations are reported in the *Table 4*.

**Table 4: Taqman probes used to quantifying mRNA level with qPCR.**  
(Abbreviations: Mm= mus musculus, Hs= Homo sapiens).

<b>TARGET</b>	<b>CODE</b>
<i>P21</i>	Mm04205640_g1
<i>SOX2</i>	Hs01053049_s1
<i>NESTIN</i>	Hs00707120_s1
<i>ELAVL2</i>	Hs00270011_m1 Mm00516015_m1
<b>REFERENCE GENES</b>	<b>CODE</b>
<i>TBP</i>	Hs00427620_m1 Mm00446973_m1
<i>HPRT1</i>	Hs01003267_m1 Mm00446968_m1
<i>B2M</i>	Hs00984230_m1 Mm00437762_m1

All probes were labelled with FAM report dye. The qPCR reaction was performed with 10ng of cDNA, with KAPA Probe Fast Universal qPCR Kit (RESNOVA, KK4702), using manufacturer's instructions. Amplifications were performed over 39 cycles, including a denaturation (95°C, 3 seconds), an annealing step (60, 20 seconds) and an extension step (72°C, 1 second), using CFX96 Real-Time PCR Detection System (Bio-Rad, 185-596). The analysis was performed on 96-well reaction plates (Bio-Rad, HSP 9645) in three biological replicates, each performed in three technical replicates, using  $2^{-\Delta\Delta Ct}$  method. Data acquisition and the analysis of the qPCR assays were performed using CFX Manager™ Software 184-5000 (Version 3.0, Bio-Rad).

#### 4.2.7 Microarray analysis

Total and polysomal RNA, obtained as described in the chapter (3.2.1-3.2.3), was hybridized on Agilent-014850 Whole Human Genome Microarray 4x44K G4112F, following Agilent protocol "One- Color Microarray-Based Gene Expression Analysis (Quick Amp Labeling)".

The hybridization results were analysed using the product of the ranks (Rank Product, RP), developed by Breitling et al., 2004 (126). Significant results (P-value <0.01) were clustered

hierarchically using the database DAVID (Database for Annotation, Visualization and Integrated Discovery) Bioinformatics Resources 6.7 .Analysis was performed in two steps. First, all the genes that were differentially expressed (Differential Expression Genes – DEGs) between a condition of control and a condition of treatment were extracted. Then, the genes differentially expressed between total mRNA and polysomal mRNA samples were determined.

#### 4.2.8 Luciferase assay

In order to determine the linear range of DNA concentration for the luciferase assays, H2b2T-HuB were transfected with several concentration of either the firefly luciferase plasmid (pGL4.13) or each of the tested reporter plasmids (see section 3.8 Plasmid construction). The concentrations tested were: 0,04; 0,06; 0,08; 0,1; 0,12 µg. This initial screen revealed that 80 ng of DNA was the best concentration for the assay. The Renilla luciferase plasmid, pGL4.74 (Promega, E6921), was co-transfected after first screening revelation of the best concentration needed, that was 30 ng of DNA. The plasmid was used as control in order to eliminate any apecific response, which is not dependent on the inserts.

Luciferase assays were performed using the Dual-GloLuciferase Assay System (Promega, E2940) 24 and 48 hours after transfection.

The experimental results ( $X$ ) was obtained with the formula:

$$X = \frac{Mean_{Firefly\ L.\ Signals}}{Mean_{Renilla\ L.\ Signals}}$$

then for each  $X$  value the error  $\Delta X$  was calculated as the Standard Deviation of the mean of each sample Firefly/Renilla ratio.

#### 4.2.9 Plasmid construction

To test whether the regulation of p21 mediated by mHuB occurs via the p21 UTRs, three plasmids were created (*Fig 4*), in which the coding region of a luciferase reporter gene was flanked by:

- 1) The 3'UTR of murine p21 plus an unrelated 5'UTR;
- 2) The 5'UTR of murine p21, variant 1, plus an unrelated 3'UTR;
- 3) The 5'UTR of murine p21, variant 2, plus an unrelated 3'UTR;

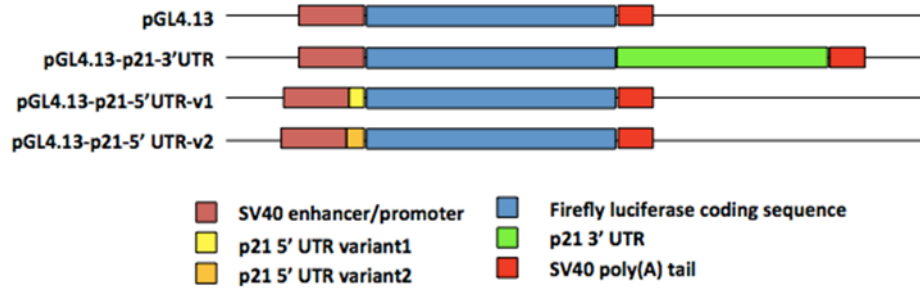


**Figure 5: structures of the created plasmids**

The parental plasmid for cloning the p21 UTRs was pGL4.13 (Promega, E668A), which encodes the luciferase reporter gene *Luc2* (derived from *Photinus pyralis*) under the regulation of the strong SV40 early enhancer/promoter. This gene is engineered to be codon-optimized for mammalian expression and consensus sequences for transcription-binding sites has been removed from regulatory regions. Therefore, the vector is designed for high expression and reduced anomalous transcription in mammalian cells and can be used as an expression control or a co-reporter vector.

#### 4.2.10-1 Generation of pGL4.13-p21-5'UTR-v1 and pGL4.13-p21-5'UTR-v2

To generate the pGL4.13 plasmids containing the p21 5'UTRs we used the following two gBlocks Gene Fragments (purchased from IDT), which contains the two variants of p21 5'UTR (highlighted in blue) flanked by *HindIII* sites (bolded and underlined):

>p21\_v1\_5'UTR

TAGCCGATATCAACAGAGTATACCAAACGGTTTGATATCGCA**AAGCTTAGC**  
**AGCCGAGAGGTGTGAGCCGCCGCGGTGTCAGAGTCTAGGGGAATTGGAGT**  
**CAGGCGCAGATCCACAGCGATATCCAGACATTCAGAGA**AAGCTT**GCGG**

>p21\_v2\_5'UTR

TAGCCGATATCTAACGTAGTAATAAACGGTTTGATATCGCA**AAGCTTGGTGG**  
**TGGAGACCTGATGATACCCAACCTACCAGCTGTGGGGTGAGGAGGAGCATG**  
**AATGGAGACAGAGACCCCAAGATAATTA**AAGGACGTCCCACTTTGCCAGCAG****  
**AATAAAAGGTGA**AAGCTT**GCGGC**

Each gBlocks was digested with *HindIII*-HF (NEB, R3104S) and ligated to the parental vector previously restricted with the same enzyme and dephosphorylated with Antarctic Phosphatase (NEB, M0289S). Ligation products were used to transform XL1-Blue competent cells (Stratagene,

200249) and the plasmid DNA of several individual transformants was extracted using a standard method (Maniatis and Sambrook, 1982). To test for the presence of an insert, the plasmid DNA from individual transformants, along with a sample of the parental vector (which served as a negative control), were digested with *ApaI* and *BglIII*. To test for the direction of the inserts, clones containing a single insert for the 5'UTR variant 1 were digested with *EcoRV* and *BglIII* (*EcoRV* is present once in the v1 insert; bolded), whereas clones containing a single insert for the 5'UTR variant 2 were digested with *MseI* (*MseI* is present once in the v2 insert; bolded).

Presence and orientation of the inserts were confirmed by DNA sequencing, using the following primer:

Lux-5'rev 5'-CTGCTCGCCGGCGGTCC-3'

#### 4.2.10-2 Generation of pGL4.13-p21-3'UTR

To generate a pGL4.13 plasmid containing the mouse p21 3'UTR, we first PCR-amplified the mouse p21 3'UTR from mouse spinal cord cDNA (kindly provided by Daniele Peroni) using the following two primers (*XbaI* sites are underlined):

p21\_3'UTR\_Fw 5'-GCGCTCTAGATTTTCTATCACTCCAAGCGCAGATTGG-3'

p21\_3'UTR\_Rv 5'-GCGCTCTAGATCATCGAGAAGTATTTATTGAGCACCAGC-3'

For the PCR reaction, it was used: 100 ng of DNA template, 1.5 µl of each primer (100 mM stock) and 5 units of high-fidelity AccuPrime Taq DNA Polymerase (Invitrogen, 12346-086) in the presence of the appropriate buffer. The PCR program was optimized as follows:

Start: 95°C for 120 sec	
Denature: 95°C for 30 sec,	} 34 cycles
Anneal: 61°C for 30 sec	
Extend: 68°C for 105 sec	
End: 68°C for 180 sec.	

After amplification, the sample was then resolved on a 1% agarose gel and the ~1.4 Kb DNA fragment was gel-purified using the Wizard SV Gel and PCR Clean-Up System (Promega, A9282). The gel-purified DNA fragment was digested with *XbaI* and ligated to a pGL4.13 vector previously

restricted with the same enzyme and dephosphorylated with Antarctic Phosphatase (NEB, M0289S). Ligation products were used to transform XL1-Blue competent cells (Stratagene, 200249) and the plasmid DNA of several individual transformants were extracted using a standard method (Maniatis and Sambrook, 1982). To test for both presence and orientation of the insert, plasmid DNA from individual transformants were restricted with *EcoRV* (*EcoRV* is present once in the parental vector and once in the 3'UTR close to one of the ends). The insert from two positive clones were completely sequenced using the following two sequencing primers:

Luc\_3'                    5'-CCGCGAGATTCTCATTAAGGCC-3'  
 SV40\_5'    5'-GGTTTGTCCAAACTCATCAATGTATC-3'

#### 4.2.11 qRT-PCR of H2b2T cells steadily expressing HuB

SYBR Green DNA-binding dye was used to detect p21 mRNA levels in H2b2TstHuB stable cell line. The primers used for the analysis were created taking into account that longer amplicons generate stronger signals (Arya et al., 2005). Thus all have about the same short length, and were:

p21\_3'UTR\_Fw                    5'-GCCTTAGCCCTCACTCTGTG-3'  
 p21\_3'UTR\_Rw                    5'-AGGGCCCTACCGTCCTACTA-3'

p21\_CDS\_Fw                    5'-CGGTGGAACCTTTGACTTCGT-3'  
 p21\_CDS\_Rw                    5'-AGAGTGCAAGACAGCGACAA-3'

p21\_5'UTRv2\_Fw                    5'-GGGTGAGGAGGAGCATGAAT-3'  
 p21\_5'UTRv2\_Rw                    5'-TATTCTGCTGGCAAAGTGGGA-3'

p21\_5'UTRv1\_Fw                    5'-CGGTGTCAGAGTCTAGGGGAA-3'  
 p21\_5'UTRv1\_Rw                    5'-GTGCCTGTGGCTCTGAATGT-3'

For this analysis the primers were designed in order to cover specific regions of p21 transcripts (5'UTR, CDS and 3'UTR), which were not available as Taqman probes. The primers were designed with Primer3Plus (<http://www.bioinformatics.nl/cgi-bin/primer3plus/primer3plus.cgi>) and verified with BLAST (<http://blast.ncbi.nlm.nih.gov/>). Primers were used at concentration of 200nM. Efficiencies were between 98 and 100 % slopes between -2,9 and -3,1, and R2 near 1. The

housekeeping gene used was *ribosomal protein L41* gene (courtesy of Giovanni Provenzano). Four biological replicates were analysed. For each biological replicate, 3 technical replicates were tested. The reaction mix for each well contained:

<i>Components</i>	<i>Volume per well</i>
2x Kapa Sybr	5 $\mu$ l
Forward primer (200nM)	0,2 $\mu$ l
Reverse primer (200nM)	0,2 $\mu$ l
cDNA (5 ng/ $\mu$ l)	2 $\mu$ l
Millipore H2O for Molecular Biology	2,6 $\mu$ l
<hr/>	
<i>Total volume</i>	10 $\mu$ l

The thermocycler used was the CFX96 Touch Real-Time PCR Detection System(Bio-Rad, 185-5196).

### **4.3 PROTEIN METHODS**

#### 4.3.1 Immunoblotting analysis

Cells were harvested after 48h with a scraper (Sarstedt, 831832). RIPA buffer (50 mM Tris HCl pH 7,4; 150 mM NaCl; 1 mM MgCl<sub>2</sub>; 0,1 % TritonX100) supplemented with, 1/100<sup>th</sup> phosphatase inhibitor cocktail 1 and 2 (Sigma, P0044 and P5726), Pepstatin A (Sigma, 77170; 1:1000 final dilution) and protease inhibitor cocktail (Sigma, P834; 1:200 final dilution), was used as lysis buffer to extract proteins. 300 $\mu$ l of lysis buffer were added to each samples, three freezing-thawing cycles (in liquid nitrogen and at 37°C, 5 minutes each cycle) were performed followed by a centrifugation at maximum speed for 30 minutes. Total protein concentration was determined using the Bradford assay (Sigma, B6916) using BSA as a protein standard. For each sample, 10  $\mu$ g of total protein were subjected to 10% SDS-Tris glycine polyacrylamide gel electrophoresis and transferred to a nitrocellulose membrane (Bio-Rad, 162-0112). The membrane was blocked with 5% nonfat milk (Santa Cruz, sc2325) in TBS-Tween buffer [10mM Tris (pH7.5), 100mM NaCl, 0.1% Tween 20 (Sigma, P2287)] and incubated with primary antibodies for 1h at room temperature. The same incubation was performed with the secondary antibodies. Detection of immunocomplexes was performed using the ECL system (GE Healthcare, RPN2232). Normalization was done using GAPDH or  $\beta$ -tubulin. The antibodies used in this study are reported in *Table 5*.

**Table 5: Antibodies used for WB analysis.**

<b><i>Protein targeted</i></b>	<b><i>Code of Antibody</i></b>	<b><i>Dilution</i></b>
<i>P21</i>	sc-397, Santa Cruz	1:200
<i>ELAVL2</i>	14008-1-AP, Proteintech	1:3000
<b><i>Reference proteins</i></b>	<b><i>Code of Antibody</i></b>	<b><i>Dilution</i></b>
<i>B TUBULIN</i>	sc-53140, Santa Cruz	1:1000

#### **4.4 STATISTICAL ANALYSES**

Statistical analysis was performed with GraphPad Prism software (GraphPad Software, San Diego, CA, USA). Statistical significance ( $***p < 0.001$ ;  $** 0.001 \geq p \leq 0.01$ ;  $* 0.01 \geq p \leq 0.05$ ) was determined using an unpaired t-test of at least three experiments.

#### **4.5 BIOINFORMATIC ANALYSIS OF GBM SAMPLES**

Copy number alteration and gene expression profiles of 372 glioblastoma multiforme (GBM) samples were downloaded from the TCGA Data Portal (95). Genes subjected to significant copy number alterations (both amplifications and deletions) were extracted from these profiles and intersected with a list of 1794 verified RBPs according to InterPro RNA-binding domains (96) and a set of novel RBPs identified in a recent work by Castello et al (97). The percentage of samples bearing a genomic alteration was extracted from the TCGA Data Portal; the fraction of samples exhibiting an over- or under-expression of each of these RBPs mRNAs was also obtained from the same source.

RBPs subjected to agreeing alterations (i.e., both amplified and overexpressed or both deleted and underexpressed) in at least 15% of the samples were eventually selected as interesting candidates.

Samples bearing genomic alterations of these RBPs loci were intersected with the GBM samples grouping as defined in Verhaak et al., (98), to identify potential association of an RBP to one of the groups. Kaplan-Meier survival curves for these candidates were computed by means of the REMBRANDT database (99), as the coverage of TCGA samples bearing alterations of these RBPs was insufficient. The logrank test p-value was then used to further refine the candidate RBPs list to the ones showing a significant survival difference between the amplified/deleted conditions.



A search for regulators and targets of these RBPs was performed by means of the AURA database (100). Eventually, Pearson correlation between the mRNA level of the candidate proteins and mRNA level of all genes was computed in order to identify putative novel targets of these RBPs.

## **5. RESULTS**

### **5.1 Genome-wide analysis of RNA binding proteins expression alterations in GBM identifies HuB as a potential tumor suppressor protein.**

To identify potentially altered translational networks in GBM, we started by correlating the genomic alteration status and related mRNA levels of RNA-binding proteins in 372 GBM samples obtained from the TCGA Data Portal (TCGA-Consortium, 2008). We reasoned that genomic amplifications or deletions affecting RBPs and leading to alterations in their protein expression levels are likely to impact their target networks in a significant way, potentially perturbing fundamental cell processes. To this aim we first identified in our GBM samples the genes subjected to significant copy number alterations (both amplifications and deletions) and determined which of these genes correspond to RBPs. Of this group, we selected the RBPs whose copy number alteration correlated with their altered expression levels in at least 15% of the samples (i.e. genes that either showed amplification and were overexpressed in our samples or were deleted and underexpressed). We therefore identified 56 RBPs subjected to agreeing alterations (i.e., both amplified and overexpressed or both deleted and underexpressed) in at least 15% of the samples. Among the 56 RBPs identified using our parameters, which are listed in Figure 1, we noticed the presence of HuB (ELAVL2) as deleted in 48% of the samples and down-regulated in more than 90% of these. Given the evidence for HuB activity as a differentiation factor in neuronal cells (25, 64), we reasoned that it may act as an oncosuppressor, therefore suggesting its loss as a required mechanism for tumor progression. Therefore, we decided to further investigate the role of HuB in glioblastoma multiforme.

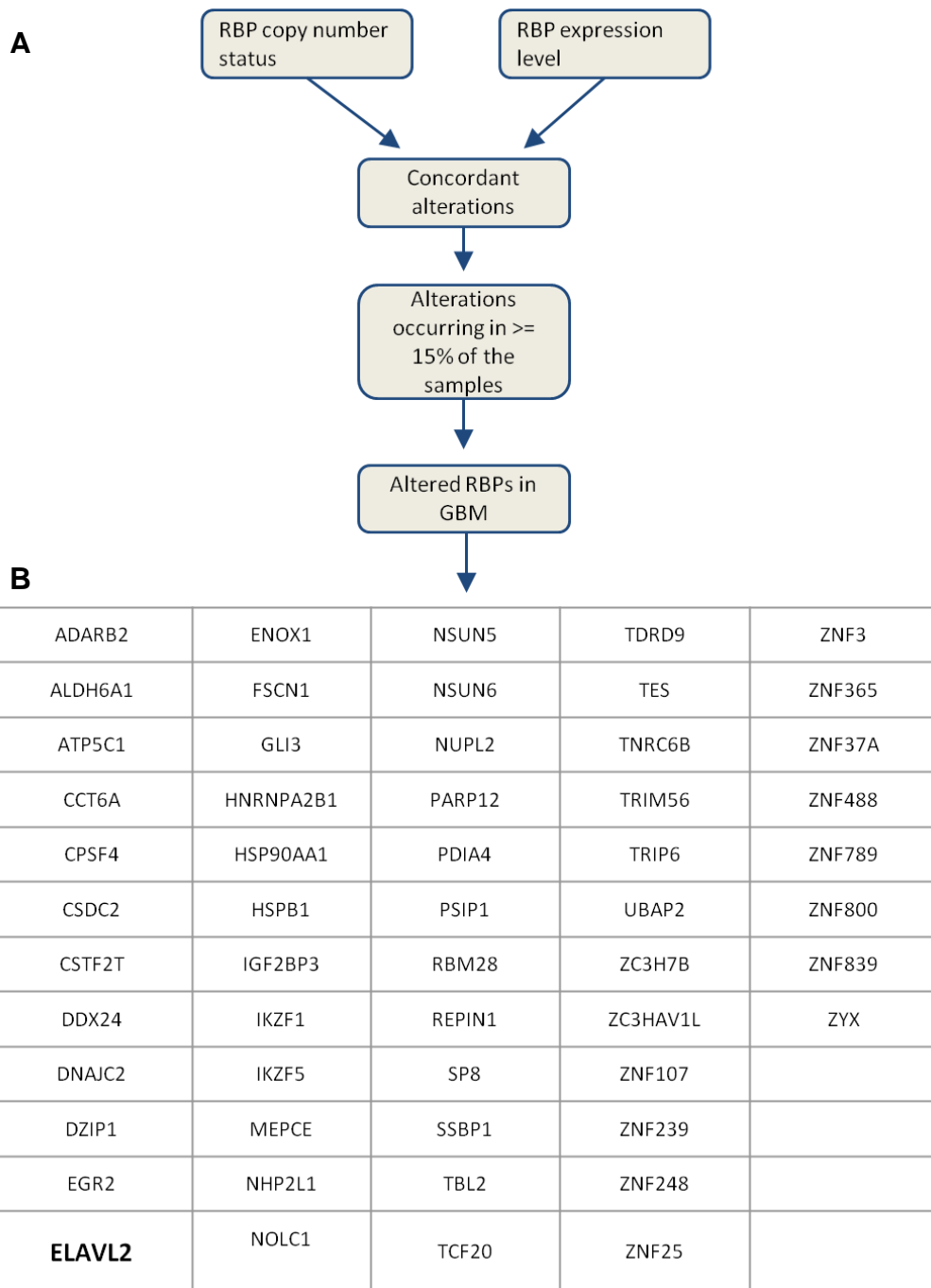


**Figure 6: Genome-wide analysis of RNA binding proteins expression alterations in GBM identifies HuB as a potential oncosuppressor protein.** (A) Pipeline used to identify altered RBPs in glioblastoma (see Material and Methods). Copy number alterations and expression changes (up/down-regulation) were combined to obtain RBPs which had concordant changes (e.g. deleted and down-regulated). RBPs conforming to this criteria were then filtered for being altered in at least 15% of all considered samples. (B) List of the 56 RBPs conforming to the criteria used in our bioinformatic analysis.

## 5.2 HuB loss is a frequent event in GBMs.

Since the bioinformatics analysis of GBM samples (Fig. 6) unraveled a possible role of ELAVL2 deletion in this cancer, we first tested whether indeed the gene is altered in human GBM biopsies by fluorescent *in situ* hybridization (FISH) analysis. FISH analysis is a standard technique for detecting the presence and frequency of chromosomal alterations in heterogeneous samples, such as human cancers. As shown in Fig. 7, we found that ELAVL2 was heterozygously deleted in about 40% of the GBM samples and was homozygously deleted in about 8% of the samples. These results are in agreement with a putative role of ELAVL2 in GBM.

Nevertheless, in 9p21.3 the ELAVL2 locus is very close to the CDKN2A locus (1.8 Mb of distance between the two loci), with only one intervening other gene locus, that for the DMRTA1 gene. Since the p16INK4A/p19ARF proteins, encoded by CDKN2A, are the most powerful and most frequently inactivated oncosuppressor loci in cancer in general (86) and in gliomas in particular (8, 9), the possibility exists that the ELAVL2 loss is simply an epiphenomenon associated to CDKN2A deletion, and does not have a role of modulator of the GBM cell phenotype.

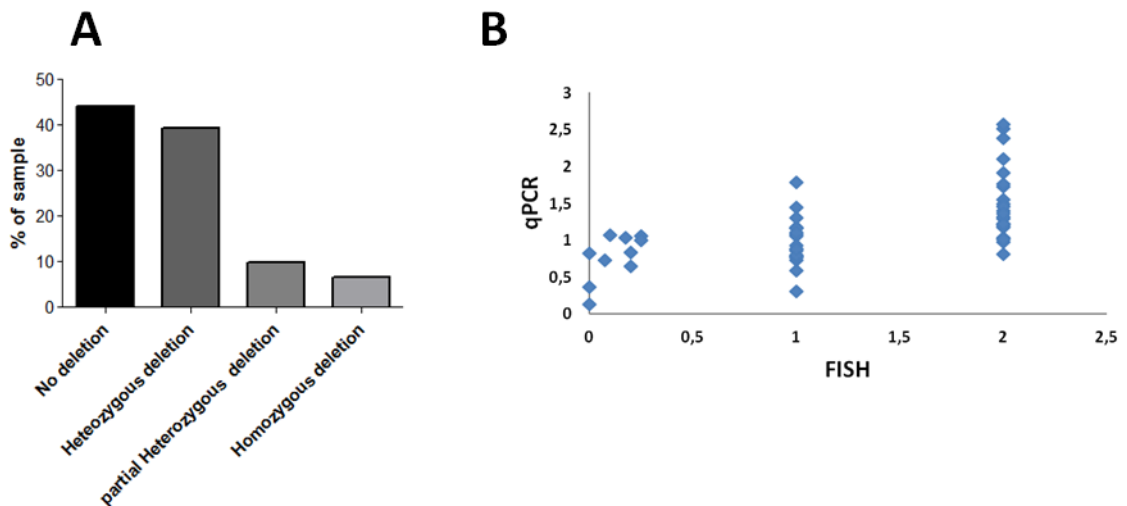


**Figure 7: HuB loss is a frequent event in GBMs.**(A) Deletion percentage found in GBM samples with FISH technique.(B) Correlation between qPCR and FISH results. “0” indicates Homozygous deletion. “1” indicates Heterozygous deletion. “2” indicates No deletion. On the X axis are reported the FISH results, whereas on Y axis are reported the qPCR results.

### **5.3 The patterns of codeletion of the CDKN2A and the ELAVL2 loci in GBM are suggestive of a modifier role of ELAVL2 loss in a CDKN2A loss background.**

ELAVL2 and cyclin-dependent kinase inhibitor 2A (CDKN2A) map at the same locus on chromosome 9 (9p21.3), at a distance of 1.8 Mb and with only one intervening gene, DMRTA1 (doublesex and mab-3-related transcription factor-like family A1). Since the p16INK4A/p19ARF proteins, encoded by CDKN2A, are powerful and frequently inactivated oncosuppressor loci in cancer in general (86) and in gliomas in particular (8, 9), the possibility existed that the ELAVL2 loss is simply an epiphenomenon associated to CDKN2A deletion, and does not have a role of modulator of the GBM cell phenotype.

Therefore, we became interested in understanding the structure of the deletion spanning the CDKN2A and the ELAVL2 loci, by studying as many GBM samples as possible. To this aim, we initially exploited the publicly available data related to The Cancer Genome Atlas (TCGA) core GBM samples (n=372), endowed with high resolution genomic imbalance profiles obtained by aCGH. Subsequently, we examined the same two loci by quantitative PCR (qPCR) on genomic DNA of an independent cohort of 233 consecutive GBM samples diagnosed between 2006 and 2009 at the Verona Borgotrento Hospital (Verona, Italy) by the same pathologist. *Figure 8A* reports synoptically the results of both analyses. We found that about half of the tumors (47% TCGA and 42% Verona samples) did not present any gain or loss in the CDKN2A and ELAVL2 loci. Deletions of ELAVL2 in the presence of wild type CDKN2A were basically absent in both sample groups, while CDKN2A monoallelic loss was accompanied in about a quarter of cases (19% TCGA and 25% Verona samples) by an intact ELAVL2, and less frequently (8% TCGA and 6% Verona samples) by a corresponding monoallelic loss of ELAVL2. Homozygous deletion of CDKN2A, the lesion at the basis of the oncosuppressor activity of p16INK4A and p19ARF, was present in about a quarter of the total samples, (26% TCGA and 38% Verona samples) of which 50-61%, depending on the sample group, were not deleted at all at the ELAVL2 locus, which instead was correspondingly deleted in the remaining cases (10%-20% of the total samples).

The only discrepancy between the two groups, which showed a remarkable agreement considering the different sampling and the different detection techniques used in evaluating the DNA copy number, was the presence, only in the Verona samples, of an high frequency of homozygous CDKN2A deletions in combination with heterozygous ELAVL2 deletions (8%). Therefore, it seems that the 1.8Mb region of 9p21.3 having these two loci at the extremes is deleted in GBMs following two patterns: the first and prevalent pattern is a focused deletion involving the CDKN2A, but not the ELAVL2 locus, while the second is a deletion extended to this second gene, found numerically in about 50% of the total CDKN2A deleted samples.

To test the possibility that this deletion pattern results from a random distribution of deletion margins and is therefore not the result of a double selective pressure on *CDKN2A* and *ELAVL2*, we looked in our GBM samples for the existence of double focal deletions affecting these two genes. To this aim, qPCR analysis testing the presence of two intervening regions (INV1 and INV2) between *CDKN2A* and *ELAVL2* was performed on the 58 GBM samples bearing homo- and/or heterozygous deletions at both loci. We found that in 12 samples (Fig. 8B) the continuity of the deletion between *CDKN2A* and *ELAVL2* is interrupted. Therefore, two independent focal deletion events occurred in 20 % of the GBM samples bearing homo- and/or heterozygous deletion at *CDKN2A* and *ELAVL2*, rendering the double focal deletion a rare, but recurrent event.

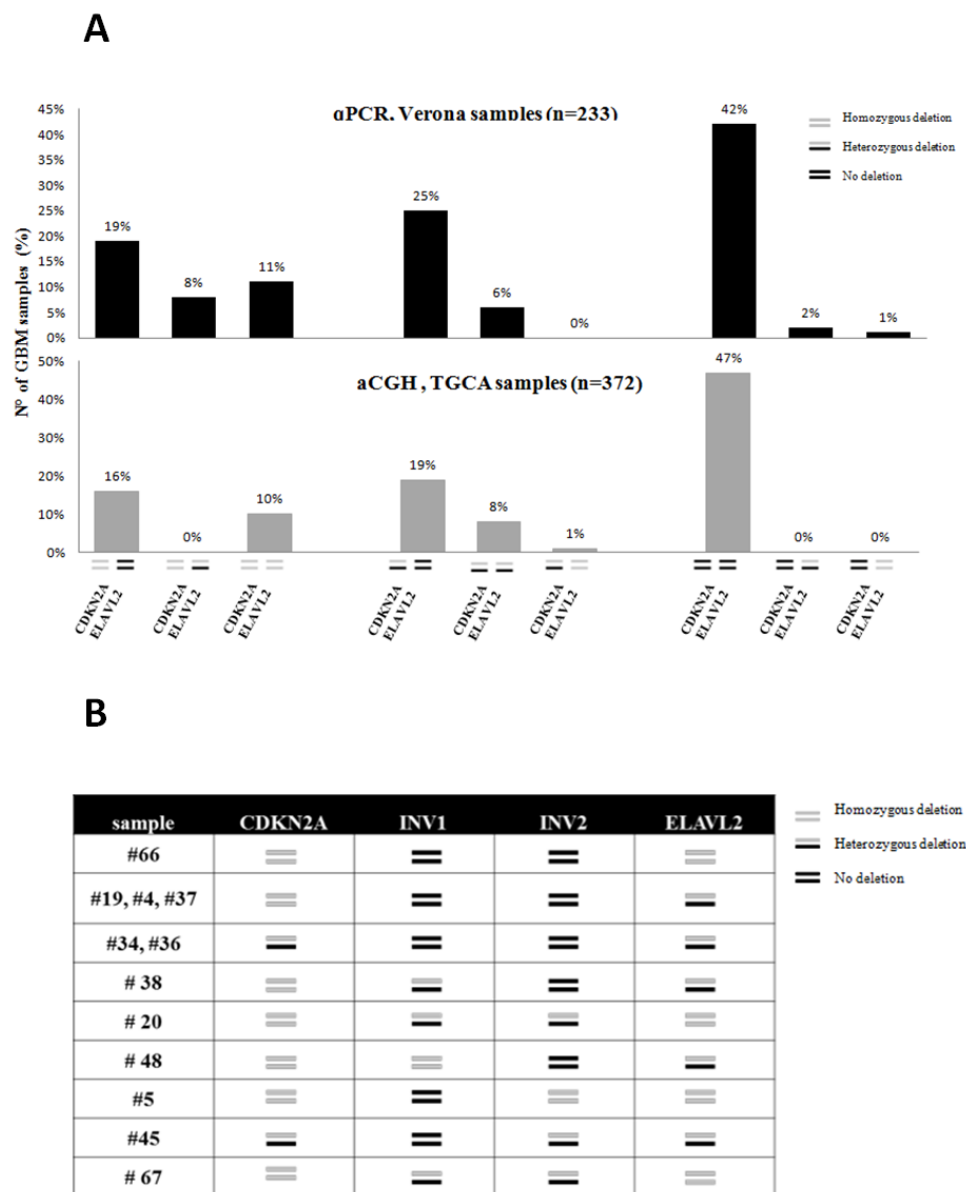


**Figure 8:** Deletion of *ELAVL2* in GBM occurs frequently and is always associated with *CDKN2A* deletion; however, in a subset of samples is the results of two independent deletion events.(A) Frequency of

deletions at the *CDKN2A* and *ELAVL2* loci in the TCGA GBM core dataset (lower panel) detected by aCGH and from paraffin-preserved GBM samples from the Verona's hospital (upper panel) detected by qPCR. Each gene is depicted by two horizontal bars; a black bar represents the presence of the allele, whereas a grey bar represents the absence of allele. (B) Deletion profiles of *CDKN2A*, *ELAVL2* and the two intervening regions (*INV1* and *INV2*) for samples bearing deletions of both *CDKN2A* and *ELAVL2*, analysed by qPCR. A black bar represents the presence of the allele, whereas a grey bar represents the absence of allele.

#### **5.4 HuB modulation in U87MG cells and HuB reconstitution in glioma initiating cells indicate that HuB suppresses glioma cell migration and invasion.**

We then looked for suitable cell models to investigate the effects of the HuB protein in a *CDKN2A* null glioma background. We initially employed U87MG cells, a commonly used glioma cell line, and we genotyped it for the two loci of our interest. U87MG cells resulted to be homozygously deleted for *CDKN2A* and heterozygously deleted for *ELAVL2* (Fig. 9A1). Downregulation of HuB by a lentivirally-transduced shRNA reduced its expression to more than 80% (Fig. 9A2), producing an HuB knock-down model. The measure of cell motility by both a scratch test (87) and by a Boyden chamber assay coherently demonstrated a statistically significant increase with reduction of HuB, which was revealed in a more pronounced way (increase of more than 60%) through the Boyden chamber (Fig. 9B1 and 9B2). In the same *ELAVL2* heterozygous background we also stably overexpressed HuB by lentiviral infection, obtaining a sharp decrease of cell motility in the Boyden chamber (Fig. 9B3).

Since stabilized cell lines are not considered entirely recapitulating glioma cell behavior (13), we also genotyped a number of primary glioma initiating cells (GICs) grown in a defined standard FGF2/EGF medium (84). We choose GIC#030616, whose cells are homozygously deleted for both *CDKN2A* and *ELAVL2* (Fig. 9A3), and therefore suitable to rescue HuB expression. Using this model, we could perform full reconstitution of HuB in a *CDKN2A* null background (Fig. 9A4-6), which again resulted in clear decrease in motility (Fig. 9B4). We therefore concluded that loss of HuB expression, both monoallelic and biallelic, is able in glioma cells which have lost p16INKA and p19ARF expression to markedly reduce motility. Moreover, there is an inverse relationship between this cell phenotype, which is highly relevant to gliomatogenesis, and HuB expression.

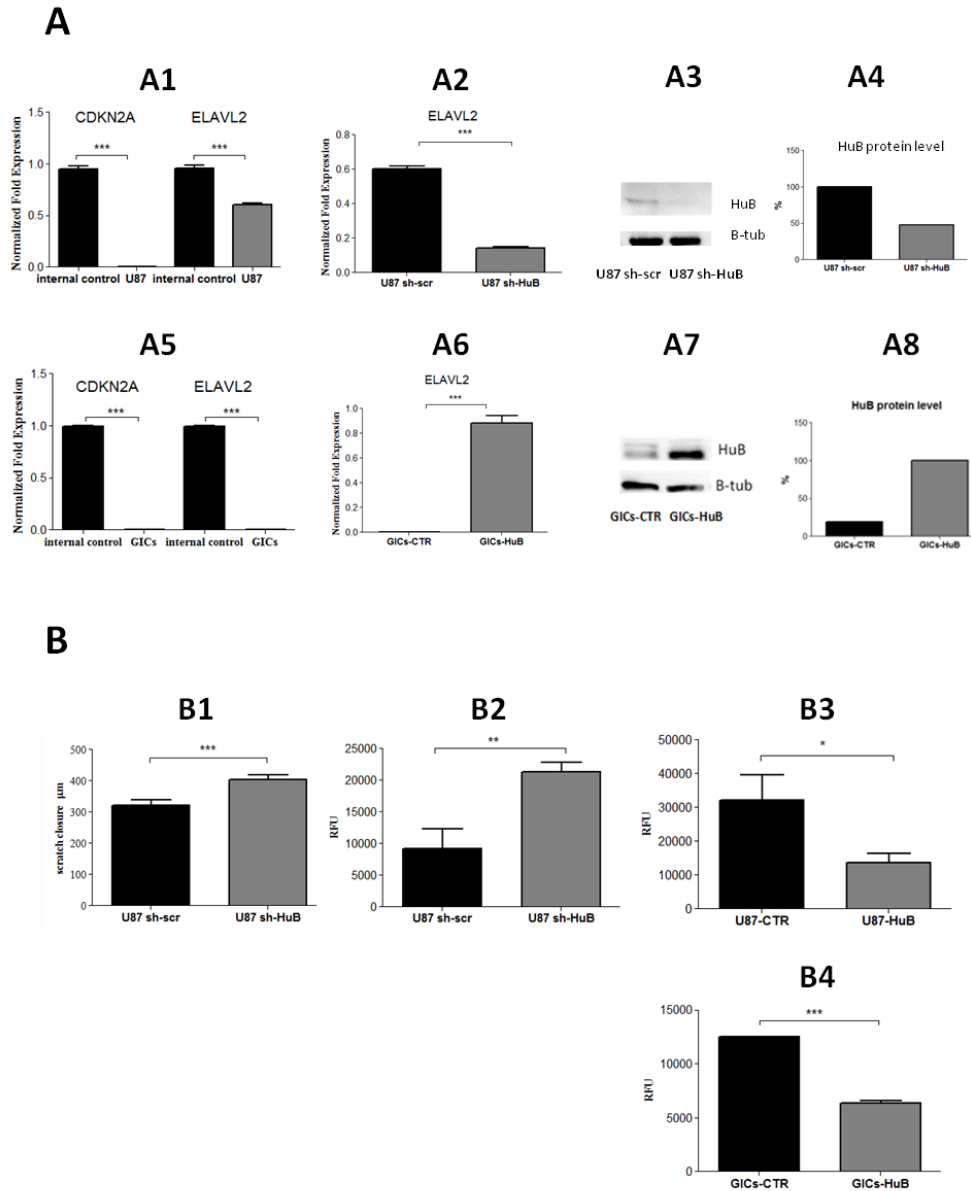


**Figure 9: ELAVL2 over-expression in two neuronal cell lines leads to a reduction in cell migration.** (A) U87 cells are heterozygous deleted for ELAVL2 and can be knock-down, whereas GICs are homozygous deleted for ELAVL2 and can be overexpressed. In A1-4 the internal control represents conditions of no deletion. Experiments were performed from three biological replicates, each one consisting of three technical replicates. Error bars indicate standard error of the mean (SEM). Asterisks indicate  $P < 0.05$  as determined by unpaired Student's *t*-test. (A1) CDKN2A and ELAVL2 copy number in U87 cells, quantified on genomic DNA using qPCR. U87 are homozygous deleted for CDKN2A and heterozygous deleted for ELAVL2. (A2) ELAVL2 expression in U87 cells knock-down (U87 sh-HuB) and control cells (U87 sh-scr), quantified with qPCR. (A3) ELAVL2 protein level in U87 sh-scr and in U87 sh-HuB as determined by immunoblotting. (A4) Quantification of the immunoblot shown in A3. (A5) CDKN2A and ELAVL2 copy number in GICs, quantified on genomic DNA using qPCR. GICs are homozygous deleted for both CDKN2A and ELAVL2. (A6) ELAVL2 expression in GICs after over-expression (GICs-HuB) and in control cells (GICs-CTR), analyzed by qPCR. (A7) ELAVL2 protein level in GICs-HuB and in GICs-CTR as determined by immunoblotting. (A8) Quantification of the immunoblot shown in A7. (B) ELAVL2 knock-down affects migration. In B1-3 U87 sh-HuB indicates ELAVL2 knockdown, whereas U87-HuB indicates ELAVL2 over-expression. (B1) Migration analysis of U87 cells performed with Scratch test. (B2-3) Migration analysis of U87 cells performed with Cell Migration



Assay. (B4) Migration analysis of GICs performed with Cell Migration Assay. GICs-HuB indicates ELAVL2 over-expression. All experiments were performed from three biological replicates, each one consisting of three technical replicates. Error bars indicate standard error of the mean (SEM). Asterisks indicate  $P < 0.05$  as determined by unpaired Student's *t*-test.

Finally, we checked in the same cell models if HuB had an effect on cell invasivity, by performing the Boyden chamber assay with a matrigel layer. U87MG cells down-regulated for HuB revealed a not statistically significant tendency to increased invasion (*Fig. 10A left*), while U87MG cells overexpressing HuB displayed a 60% reduction in their invasive capabilities (*Fig. 10A right*). The difference in extent of the two results could be justified by the already low level of constitutive HuB expression in U87MG cells, because of expression of a single allele, and by the partial HuB suppression by shRNA (see *Fig. 9A2*). Reconstitution of HuB expression in GIC#030616 cells resulted in a sharp decrease in invasivity, comparable to the effect of HuB over-expression observed in U87MG cells (*Fig. 10B*).

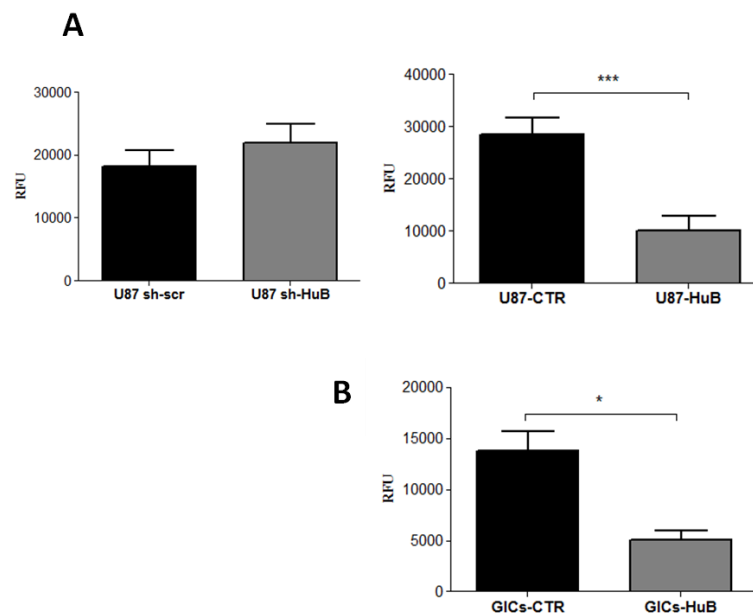


**Figure 10: ELAVL2 over-expression decreases invasion capabilities in GICs and U87 cells.** (A) The panel shows the effects of ELAVL2 knock-down (U87 sh-HuB; left) and over-expression (U87-HuB; right) on the invasion capabilities of U87 cells, as determined by the Cell Invasion Assay (see Material and Methods). (B) Effects of ELAVL2 over-expression (GICs-HuB) on the invasion capabilities of GICs, as determined by the Cell Invasion Assay. All experiments were performed from three biological replicates, each one consisting of three technical replicates. Error bars indicate standard error of the mean (SEM). Asterisks indicate  $P < 0.05$  as determined by unpaired Student's *t*-test.

### **5.5 Loss of HuB expression increases the degree of stemness in glioma cells.**

Having observed a reduction in migration and invasiveness upon HuB expression in both glioblastoma cell line models, we further tested in the same lines the ability of HuB to modulate neurosphere formation in a defined medium, a feature associated with glioma aggressiveness (94). U87MG cells increased neurosphere formation upon HuB down-regulation, and strongly decreased it by HuB up-regulation (*Fig. 11A*, top panel). Reconstitution of HuB expression in GICs determined a drastic decrease in the ability to form neurospheres, and these neurospheres were of smaller size as determined by measuring the average diameter and area with an high-content imaging system (*Fig. 11A*, middle and lower panels).

These experiments clearly indicate that HuB contribute in reducing the cells proliferation abilities in both glioma models. Neuronal development is promoted by several transcription factors including of the stemness markers nestin and SOX2 (89-94). Therefore, we tested the expression levels of these two stemless marked upon HuB down-regulation in U87 cells and expression in GICs. As shown in *Fig. 11B*, HuB down-regulation in U87MG cells resulted in a net increase of the expression of nestin and SOX2, whereas HuB expression in the HuB-deficient GICs decreased both markers (*Fig. 11B*).

Overall, these results support the hypothesis that HuB acts as an oncosuppressor, reducing the cell's ability to proliferate. This repression activity is mediated, at least in part, by a reduction in the expression of stemness genes, such as nestin and SOX2.

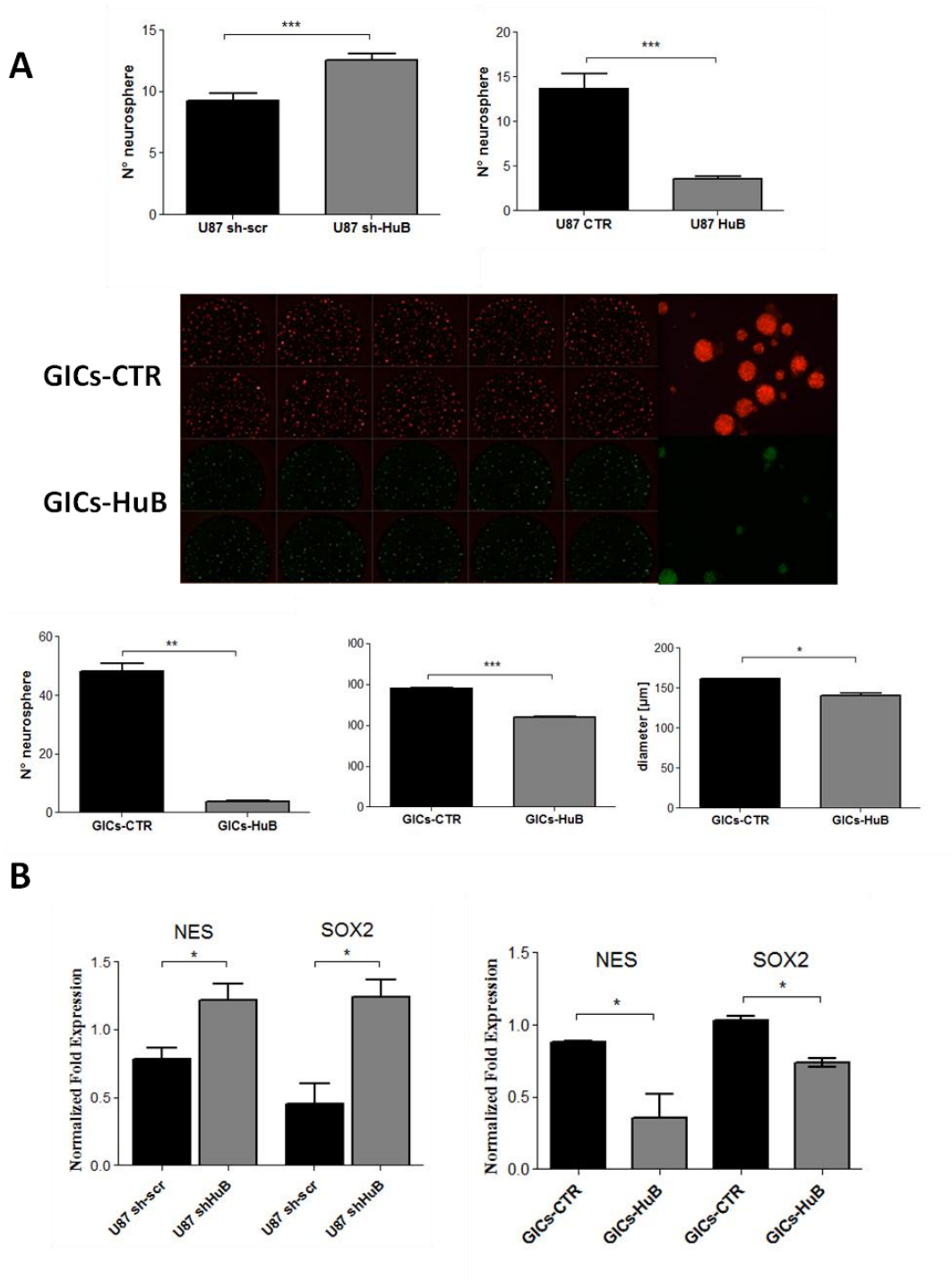


**Figure 11: ELAVL2 overexpression in GICs and U87 cells leads to a drastic decrease in neurosphere formation capabilities and lower levels of stemness markers.**(A) ELAVL2 over-expression decreases the capacity to form neurospheres. Upper panel Effects of ELAVL2 knock-down (U87 sh-HuB; left) and over-expression (U87-HuB; right) on the ability to form neurospheres in U87 cells, as determined by the Neurosphere assay (see Material and Methods). Middle panel Effects on neurosphere formation of ELAVL2 over-expression (GICs-HuB; green) or over-expression of a control plasmid (GICs-CTR; red) in GICs as determined using the PerkiElmer Operetta High-content Screening System (see Material and Methods). Ten random fields and a blow up of a representative field are shown for each condition. Lower panel Number (left), area (middle) and diameter (right) of neurospheres from the experiment shown in the middle figure as obtained from the Operetta software. All experiments were performed from three biological replicates,

each one consisting of ten technical replicates. Error bars indicate standard error of the mean (SEM). Asterisks indicate  $P < 0.05$  as determined by unpaired Student's *t*-test. **(B)** ELAVL2 levels affects stemness in GICs and U87 cells. Left panel Nestin (NES) and SRY (sex determining region Y)-box 2 (SOX2) expression levels in ELAVL2 knock-down U87 cells (U87 sh-HuB) and in control cells (U87 sh-scr) as determined by qPCR. Right panel NES and SOX2 expression levels in GICs overexpressing ELAVL2 (GICs-HuB) and in control cells (GICs-CTR) as determined by qPCR. All experiments were performed from three biological replicates, each one consisting of three technical replicates. Error bars indicate standard error of the mean (SEM). Asterisks indicate  $P < 0.05$  as determined by unpaired Student's *t*-test.

### **5.6 HuB controls the expression of genes involved in cell adhesion and motility.**

Down-regulation of HuB in U87MG cells reduced its expression to more than 80% (*Fig. 9A2*), giving the possibility to investigate the whole network of genes regulated by HuB in glioblastoma. Therefore, we performed an array-based transcriptome profiling by hybridizing polysomal mRNAs from U87MG sh-HuB or control cells (U87MG sh-scr) to a whole human genome microarray and identified all genes differentially present on polysomes between the two samples. We chose to determine the changes in the ribosomally-loaded mRNAs instead of the total mRNA changes, because there is usually a wide degree of uncoupling between the two (88) and because we were interested in assessing the effects of an RBP deleted in glioma on translational control, the level of gene expression regulation closest to the phenotype. Besides a strong signature related to cytokine activation and another to angiogenesis, we found that down-regulation of HuB affected major processes related to cell movements (cell adhesion, regulation of cell migration, locomotor behaviour and chemotaxis), for a total of 123 genes, together with the well-known phenomenon already associated to HuB, neuronal differentiation (see *Figure 12*).

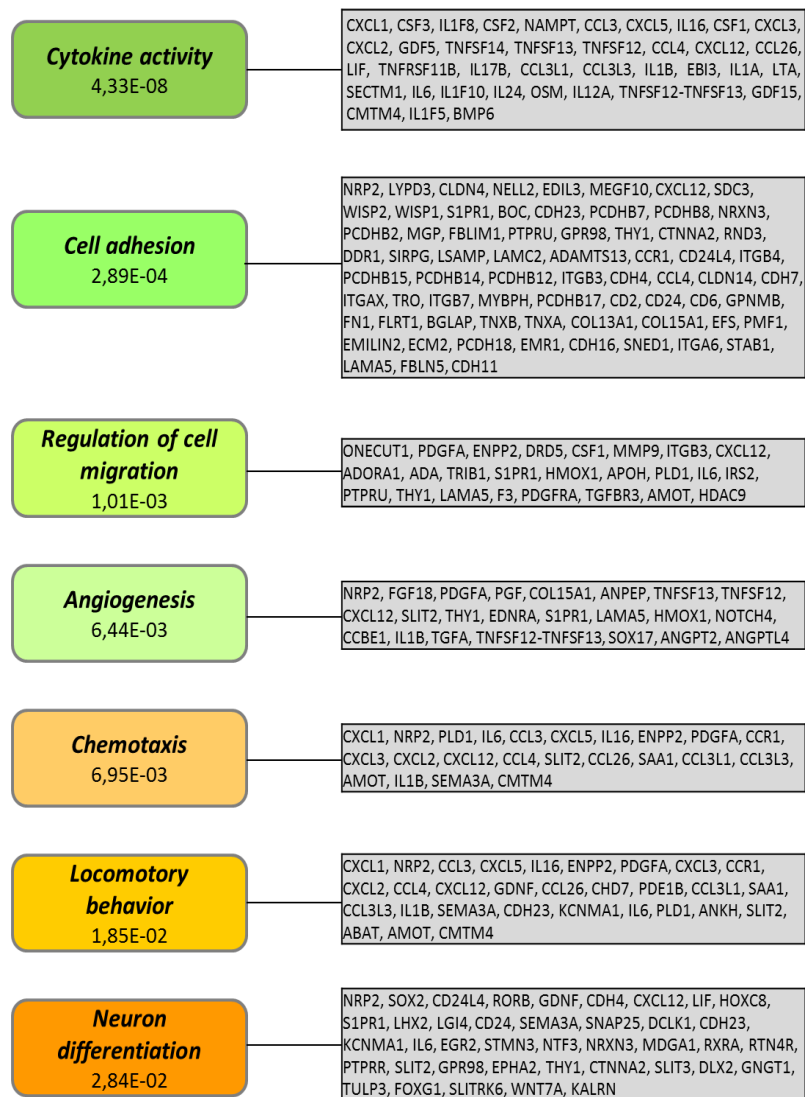


**Figure 12: HuB down-regulation impacts on functions and processes relevant to cancer progression.** The figure displays the biological processes and functions enriched in genes differentially expressed at the polysomal level following HuB down-regulation. Genes related to each term are displayed on the right side with the related enrichment p-value.

### **5.7 The p21 tumor suppressor is translationally enhanced by HuB in mouse neural tube cells.**

HuB expression in glioma stem cells resulted in a marked inhibition of clonality, i.e. an inhibition of stem cell proliferation, suggesting that it might alter cell-cycle regulation. Cyclin-dependent kinase inhibitor 1 (p21/WAF), is a known tumor suppressor gene which is indirectly transcriptionally targeted in glioblastomas by both inactivating mutations in TP53 and overexpression of BMI1 (116, 117). To test whether p21 could be a target of HuB in condition of normal neuroblast proliferation we used H2b2T cells, a line of neural tube neuroblasts derived by transgenic mice expressing the SV40 Large T antigen, and therefore able to grow indefinitely by the ability to bypass the G1-S checkpoint. They express the ubiquitous ELAVL protein HuR, but not the neuronal members of the family (HuB, HuC, HuD), therefore they are an ideal system to study HuB effects without confounding variables. We transiently transfected H2b2T cells with mouse HuB and checked the steady-state levels of p21 mRNA (*Fig. 13A*) by qRT-PCR with a probe recognizing both annotated transcript variants, which differ only for an alternative 5'UTR. Since we did not detect any changes in p21 mRNA levels, we determined the levels of the two transcript variants by qPCR using primers specific to the two 5'UTRs as well as the common 3'UTR (*Fig. 13B*), finding again no significant variation in the levels of both mRNA isoforms, in the absence or presence of transfected mouse HuB. We concluded that HuB has not effects on the steady state levels of the two annotated isoforms of p21 mRNA in neural tube cells. Then, we determined the levels of p21 protein and found a reproducible increase upon HuB over-expression (*Fig. 13C*). These results suggest that the increase of p21 protein levels induced by transient HuB expression is likely due to a translational enhancement exerted on the p21 mRNA.

To further investigate this activity, we generated H2b2T cells that stably-express HuB (H2b2t st-HuB) or control cells (H2b2t st-CTR) and transiently transfected with luciferase reporters bearing the two variants of the murine p21 5'UTRs inserted upstream of the coding sequence as well as the p21 3' UTR inserted downstream of the CDS. Luciferase activity from the firefly luciferase chimeric reporters was measured in cells stably-expressing HuB or in control cells that do not and the results were normalized to the renilla luciferase activity obtained from a co-transfected plasmid. The luciferase activities of the reporters bearing either the p21 3'UTR or the p21 5'UTR of transcript variant 1 were significantly increased in the presence of HuB, whereas no effects were seen with the p21 5'UTR of transcript variant 2 (*Fig. 13C*). Therefore, we conclude that the 5' UTR variant 1 and the 3'UTR of p21 are targeted by HuB to determine an increased p21 translation in neural tube neuroblasts.

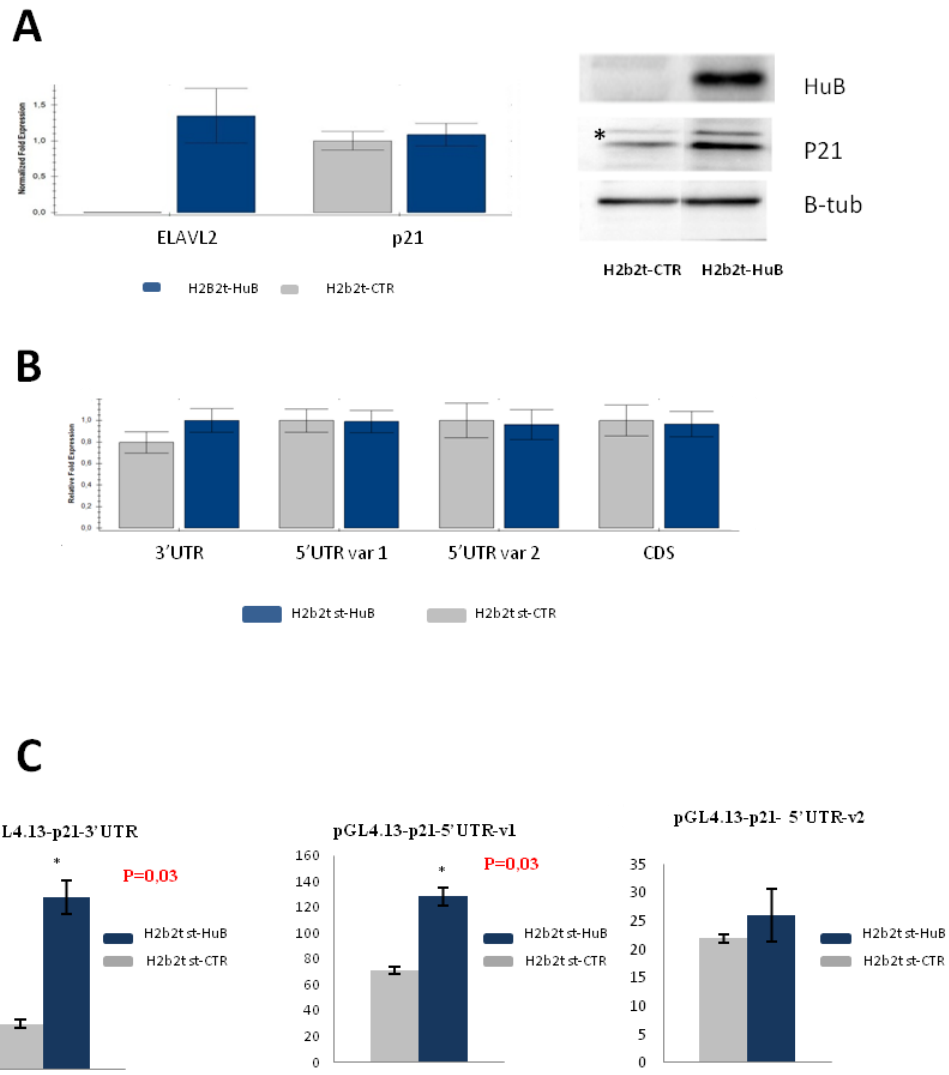


**Figure 13: p21 is regulated at post-transcriptional level by HuB, through 5' and 3'UTR binding.**(A) Over-expression of HuB in H2b2T cells. Left panel: qPCR with for HuB and p21 mRNA from H2b2T cells transiently-transfected with an expression plasmid for HuB (blue histograms) or control cells transfected with an empty plasmid (grey histograms). The high standard deviation in HuB expression levels is due to the intrinsic variability of transient transfection. The data represents four biological replicates, each one consisting of three technical replicates. Middle panel: HuB protein and p21 protein levels in H2b2T cells transiently-transfected with an expression plasmid for HuB (H2b2T-HuB) or an empty plasmid (H2b2T-CTR). The picture was taken using by ChemiDoc XRS+ System (Bio-Rad, 170-8265). As loading control, the same blot was probed for  $\beta$ -Tubulin (top). (B) Effects of HuB overexpression on p21 mRNA and protein levels. Left panel: qPCR on cells stably-expressing HuB (H2b2Tst-HUB; blue histograms) or control cells (H2b2Tst-CTR; grey histograms), using primers specific for different regions of the p21 mRNA: results from the first biological replicate (four biological replicates, each one consisting of three technical replicates). (C) HuB up-regulates p21 protein expression interacting with the p21 3'UTR as well as the 5' UTR of one of its transcript variants. *Panels*: Luciferase activity of reporters containing the p21 3'UTR (left Panel), p21 5'UTR-v1 (middle Panel) or p21 5'UTR-v2 (Right Panel) fused to the coding sequence of Luc2 gene, transiently transfected into H2b2T-HUB (blue histograms) or H2b2T-empty (grey histograms) cells. The luciferase values represent a ratio between the firefly luc and the renilla luc and represent the average of three replicates. Error bars indicate standard error of the mean (SEM). Asterisks indicate  $P < 0.05$  as determined by unpaired Student's t-test.

## **6. DISCUSSION**

The results presented here demonstrate that HuB is deleted in a fraction of GBM patients and that such deletion is correlated with a more aggressive tumorigenic phenotype. These results are relevant because, until now, it is the first study involving HuB and cancer.

HuB is a member of the ELAV family, a group of RNA binding proteins involved in neuronal differentiation. Among the four ELAV proteins, which share high levels of sequence and structure identity, the ubiquitously expressed HuR protein is the best studied. HuR is often over-expressed in human gliomas and its pharmacological inhibition results in glioma cell growth inhibition suggesting that HuR-mediated dysregulation of protein stability is necessary to sustain the rapid growth of this type of cancer (119). It appears to exert its oncogenic effects via stabilization of a subset of mRNAs, such as IL-8, VEGF and all *bcl-2* family members (120, 121).

In this study we exploited the public data on TCGA Data Portal (TCGA-Consortium, 2008) to correlate the genomic alteration status and related mRNA levels of RNA-binding proteins in 372 GBM samples, discovering that HuB is deleted in 48% of the samples and down-regulated in more than 90% of these. Given the evidence for HuB activity as a differentiation factor in neuronal cells (25, 64), we reasoned that it may act as an oncosuppressor. This result was further confirmed with FISH and qPCR techniques, performed on 233 DNA samples of GBM. We found that ELAVL2 was heterozygously deleted in about 40% of the GBM samples and was homozygously deleted in about 8% of the samples using FISH technique; whereas using qPCR it was deleted respectively in 27% and 11 % of the samples.

Nevertheless, in 9p21.3 the HuB locus (represented by ELAVL2) is very close to the CDKN2A locus (1.8 Mb of distance between the two loci), with only one intervening gene: DMRTA1, which is supposed to be involved in sexual development but not with cancer (<http://www.phosphosite.org/proteinAction.do?id=1290356&showAllSites=true>). Since the p16INK4A/p19ARF proteins, encoded by CDKN2A, are the most powerful and most frequently inactivated oncosuppressor loci in cancer in general (86) and in gliomas in particular (8, 9), the possibility exists that the ELAVL2 loss is simply an epiphenomenon associated to CDKN2A deletion, and does not have a role of modulator of the GBM cell phenotype. To this aim, qPCR analysis testing the presence of two intervening regions (INV1 and INV2) between CDKN2A and ELAVL2 was performed on the 58 GBM samples bearing homo- and/or heterozygous deletions at both loci. We found that in 12 samples the continuity of the deletion between CDKN2A and ELAVL2 is interrupted. Therefore, two independent focal deletion events occurred in 20 % of the GBM samples bearing homo- and/or heterozygous deletion at CDKN2A and ELAVL2, rendering



the double focal deletion a rare, but recurrent event. This finding strengthens the notion that in a fraction of GBM patients, HuB loss contributes to malignant tumour progression. To our knowledge, this is the first report suggesting that a selective pressure exists to eliminate two tumour suppressor genes independently in such a small genomic region. To test the hypothesis that HuB acts as an oncosuppressor, we modulated HuB protein levels in U87MG cells line and expressed it in glioma initiating cells. The results demonstrate that HuB expression suppresses glioma cell migration and invasion, whereas other studies demonstrated that ectopic misexpression of HuB in the mouse neural tube determines the appearance of neuronal markers (55). Finally we demonstrate that loss of HuB in the same cell models increases the degree of stemness, and it was further confirmed testing the expression levels of Sox2 and Nes , two well known stemness markers (89, 94). Taken together these results support the hypothesis that HuB acts as an oncosuppressor reducing cell ability to proliferate and invade.

To investigate the whole network of genes regulated by HuB in GBM, we performed an array-based transcriptome profiling by hybridizing polysomal mRNAs from U87MG sh-HuB or control cells. We found that down-regulation of HuB affected major processes related to cell movements, such as cell adhesion, regulation of cell migration, locomotor behaviour and chemotaxis and, according with the current literature, neuronal differentiation process. These results are in agreement with the previous in vitro experiments.

The most extensively studied member of ELAVL family is HuR. It is expressed early in neurogenesis (29) and acts by stabilizing a number of target mRNAs, mainly via interaction with a well characterized sequence motif in their 3' UTRs (44). This motif is present in many short-lived mRNAs and is called the de-stabilizing adenylate/uridylylate-rich element (ARE). Recent findings showed that HuR mRNA exists in three different isoforms, two of which are expressed in neurons: 2.4-kb isoform that is also ubiquitously expressed in other tissue types, and a 6.0-kb isoform that is induced during neuronal differentiation and appears to be neuron-specific. Neuronal HuB, HuC and HuD, as well as HuR itself can bind the 2.4-kb mRNA polyadenylation site, and when overexpressed, they can induce expression of an extended HuR 3' UTR that is translationally suppressed. This suggests a model where the regulation of HuR protein expression allows neurons to post-transcriptionally regulate mRNAs encoding factors required for proliferation versus differentiation to facilitate neuronal differentiation (122). In the light of the above findings, it is possible to speculate that upon the HuB loss in GBM patients, HuR expression cannot be efficiently down-regulated, which keeps cells locked in a high stemness state. To understand if this is the case, future work will focus on investigating the expression level of the different HuR isoforms upon HuB over-expression in GICs.

In search of HuB mRNA targets that would explain the functional findings, p21 was identified. We found that the 5' UTR variant 1 and the 3'UTR of p21 are targeted by HuB determining an increased p21 translation in neural tube neuroblasts. This is consistent with other studies that already identified p21 as targets of HuD (123) and HuR (71, 108), however, different cell cycle regulatory mechanisms appear to exist depending on stimuli (124). p21 is a key regulator of cell cycle and deletion of p21 in mice produces a proliferation burst of neural stem cells in the forebrain, followed by exhaustion and depletion (125), supporting the notion that p21 stabilisation by HuB could be key to induce neuronal differentiation and cell cycle arrest.

It will be interesting to analyze in detail the expression of HuR and other potential protein targets of HuB. Although it was clear from our result that a previously unrecognized lesion, the loss of the ELAVL2 locus coding for the neural RNA binding protein (RBP) HuB, could impact SVZ neurogenesis, interfering both with the exit from cell cycle and with the first phase of neuronal differentiation, and consequently being central to gliomagenesis in a fraction of GBM tumours.

## **7. BIBLIOGRAPHY**

1. *The 2007 WHO Classification of Tumours of the Central Nervous System*. David N. Louis, Hiroko Ohgaki, Otmar D. Wiestler, Webster K. Cavenee, Peter C. Burger, Anne Jouvett, Bernd W. Scheithauer, and Paul Kleihues. *Acta Neuropathol*. 2007 August; 114(2): 97–109. Published online 2007 July 6. doi: 10.1007/s00401-007-0243-4
2. *Radiotherapy plus concomitant and adjuvant temozolomide for glioblastoma*. Stupp R, Mason WP, van den Bent MJ, Weller M, Fisher B, Taphoorn MJ, Belanger K, Brandes AA, Marosi C, Bogdahn U, Curschmann J, Janzer RC, Ludwin SK, Gorlia T, Allgeier A, Lacombe D, Cairncross JG, Eisenhauer E, Mirimanoff RO; European Organisation for Research and Treatment of Cancer Brain Tumor and Radiotherapy Groups; National Cancer Institute of Canada Clinical Trials Group. *N Engl J Med*. 2005 Mar 10;352(10):987-96.
3. *Temozolomide: a review of its discovery, chemical properties, pre-clinical development and clinical trials*. Newlands ES, Stevens MF, Wedge SR, Wheelhouse RT, Brock C. *Cancer Treat Rev*. 1997 Jan;23(1):35-61.
4. *Phase II trial of temozolomide plus o6-benzylguanine in adults with recurrent, temozolomide-resistant malignant glioma*. Friedman, HS; Jiang, SX; Reardon, DA; Desjardins, A; Vredenburgh, JJ; Rich, JN; Gururangan, S; Friedman, AH et al. (March 2009). *J. Clin. Oncol*. 27 (8): 1262–7. PMID 19204199.
5. *Primary and secondary glioblastomas: from concept to clinical diagnosis*. Kleihues P, Ohgaki H, *Neuro Oncol*. 1999 January; 1(1): 44–51.
6. *Genetic Pathways to Primary and Secondary Glioblastoma*. Hiroko Ohgaki and Paul Kleihues *Am J Pathol*. 2007 May; 170(5): 1445–1453
7. *Genetic pathways to glioblastoma: a population-based study*. Ohgaki H, Dessen P, Jourde B, Horstmann S, Nishikawa T, Di Patre PL, Burkhard C, Schüler D, Probst-Hensch NM, Maiorka PC, Baeza N, Pisani P, Yonekawa Y, Yasargil MG, Lütolf UM, Kleihues P *Cancer Res*. 2004 Oct 1;64(19):6892-9.
8. *Malignant Glioma: Lessons from Genomics, Mouse Models, and Stem Cells*. Jian Chen, Renée M. McKay, and Luis F. Parada *Cell*. 2012 March 30; 149(1): 36–47.
9. *Comprehensive genomic characterization defines human glioblastoma genes and core pathways TCGA 2008*. *Nature*. 2008 October 23
10. *An Integrated Genomic Analysis of Human Glioblastoma Multiforme*, D. Williams Parsons, *Science*. 2008
11. *Stem cell, cancer, and cancer stem cells*. Tannishtha Reya, Sean J. Morrison, Michael F. Clarke & Irving L. Weissman, *Nature* 414, 105-111
12. *Identification of cancer stem cell in human brain tumors*. Singh SK, Clarke ID, Terasaki M, Bonn VE, Hawkins C, Squire J, Dirks PB. *Cancer Res*. 2003 Sep

13. *Brain tumor stem cells*. Vescovi AL, Galli R, Reynolds BA. *Nat Rev Cancer*. 2006 Jun
14. *Cancer Stem Cells—Perspectives on Current Status and Future Directions: AACR Workshop on Cancer Stem Cells*. Michael F. Clarke<sup>1</sup>, John E. Dick<sup>2</sup>, Peter B. Dirks<sup>3</sup>, Connie J. Eaves<sup>4</sup>, Catriona H.M. Jamieson<sup>5</sup>, D. Leanne Jones<sup>6</sup>, Jane Visvader<sup>7</sup>, Irving L. Weissman<sup>8</sup>, and Geoffrey M. Wahl<sup>6</sup>, *Cancer Res*. 2006 Oct 1
15. *Identification of human brain tumour initiating cells*. Singh SK, Hawkins C, Clarke ID, Squire JA, Bayani J, Hide T, Henkelman RM, Cusimano MD, Dirks PB, *Nature*. 2004 Nov 18
16. *Cancer stem cells in nervous system tumors*. Singh SK, Clarke ID, Hide T, Dirks PB. *Oncogene*. 2004 Sep 20
17. *Live-animal tracking of individual haematopoietic stem/progenitor cells in their niche*. Lo Celso C, Fleming HE, Wu JW, Zhao CX, Miake-Lye S, Fujisaki J, Côté D, Rowe DW, Lin CP, Scadden DT. *Nature*. 2009 January 1;
18. *A perivascular niche for brain tumor stem cells*. Calabrese C, Poppleton H, Kocak M, Hogg TL, Fuller C, Hamner B, Oh EY, Gaber MW, Finklestein D, Allen M, Frank A, Bayazitov IT, Zakharenko SS, Gajjar A, Davidoff A, Gilbertson RJ. *Cancer Cell*. 2007 Jan;11(1):69-82.
19. *Evidence for label-retaining tumour-initiating cells in human glioblastoma*. Deleyrolle LP, Harding A, Cato K, Siebzehnrubl FA, Rahman M, Azari H, Olson S, Gabrielli B, Osborne G, Vescovi A, Reynolds BA. *Brain*. 2011 May
20. *Expression of the stem cell marker CD133 in recurrent glioblastoma and its value for prognosis*. Pallini R, Ricci-Vitiani L, Montano N, Mollinari C, Biffoni M, Cenci T, Pierconti F, Martini M, De Maria R, Larocca LM. *Cancer*. 2011 Jan 1;
21. *CD133(+) and CD133(-) glioblastoma-derived cancer stem cells show differential growth characteristics and molecular profiles*. Beier D, Hau P, Proescholdt M, Lohmeier A, Wischhusen J, Oefner PJ, Aigner L, Brawanski A, Bogdahn U, Beier CP. *Cancer Res*. 2007 May 1;67(9):4010-5
22. *Transcription factors: from enhancer binding to developmental control*. Spitz F, Furlong EEM. *Nat. Rev. Genet*. 2012;13:613–626.
23. *mRNA localization: gene expression in the spatial dimension*. Martin KC, Ephrussi A. *Cell* 2009
24. *Post-transcriptional trafficking and regulation of neuronal gene expression*. Goldie BJ, Cairns MJ. *Molecular Neurobiology* 2012
25. *Defining a neuron: neuronal ELAV proteins*. Pascale A, Amadio M, Quattrone A. *Cellular and molecular life sciences* 2008
26. *A hierarchy of Hu RNA binding proteins in developing and adult neurons* Okano HJ, Darnell RB. *J Neurosci*. 1997 May 1;17(9):3024-37.

27. *A conserved family of elav-like genes in vertebrates* Good, P. J. (1995).. Proc.Nat. Acad. Sci. USA 92, 4557-4561
28. *Structural comparison of zebrafish Elav/Hu and their differential expressions during neurogenesis.* Park, H.C., Hong, S.K., Kim, H.S., Kim, S.H., Yoon, E.J., Kim, C.H., Miki, N., Huh, T.L., 2000. Neurosci. Lett
29. *Xenopus elav-like genes are differentially expressed during neurogenesis.* Perron, M., Furrer, M.P., Wegnez, M., Theodore, L., 1999. Mech. Dev. 84, 139–142.
30. *Sequential expression and role of Hu RNA-binding proteins during neurogenesis* Wakamatsu, Y., Weston, J.A., 1997.. Development 124, 3449–3460
31. *The 36-kilodalton embryonic-type cytoplasmic polyadenylation element-binding protein in Xenopus laevis is ElrA, a member of the ELAV family of RNA-binding proteins.* Wu, L., Good, P.J., Richter, J.D., 1997. Mol. Cell. Biol. 17, 6402–6409
32. *The expression of the Hu (paraneoplastic encephalomyelitis/sensory neuronopathy) antigen in human normal and tumor tissues.* Dalmau, J., Furneaux, H.M., Cordon-Cardo, C., Posner, J.B., 1992. Am. J. Pathol. 141, 881–886
33. *Cytoplasmic localization is required for the mammalian ELAV-like protein HuD to induce neuronal differentiation.* Kasashima, K., Terashima, K., Yamamoto, K., Sakashita, E., Sakamoto, H., 1999. Genes Cells 4, 667–683.
34. *Mammalian homologs of Drosophila ELAV localized to a neuronal subset can bind in vitro to the 3' UTR of mRNA encoding the Id transcriptional repressor.* King, P.H., Levine, T.D., Fremeau Jr., R.T., Keene, J.D., 1994. J. Neurosci. 14, 1943–1952
35. *Cloning and characterization of HuR, a ubiquitously expressed Elav-like protein.* Ma, W.J., Cheng, S., Campbell, C., Wright, A., Furneaux, H., 1996.. J. Biol. Chem. 271,8144–8151.
36. *A hierarchy of Hu RNA binding proteins in developing and adult neurons.* Okano, H.J., Darnell, R.B., 1997. J. Neurosci. 17, 3024–3037
37. *Two different RNA binding activities for the AU-rich element and the poly(A) sequence of the mouse neuronal protein mHuC .*Abe, R., Sakashita, E., Yamamoto, K., Sakamoto, H., 1996.. Nucleic Acids Res. 24, 4895–4901
38. *Poly(A) tail length-dependent stabilization of GAP-43 mRNA by the RNA-binding protein HuD.* Beckel-Mitchener, A.C., Miera, A., Keller, R., Perrone-Bizzozero, N.I., 2002. J. Biol. Chem. 277, 27996–28002.
39. *Purification and properties of HuD, a neuronal RNA-binding protein .*Chung, S., Jiang, L., Cheng, S., Furneaux, H., 1996. J. Biol. Chem. 271, 11518–11524.
40. *HuD RNA recognition motifs play distinct roles in the formation of a stable complex with AU-rich RNA.* Park, S., Myszka, D.G., Yu, M., Littler, S.J., Laird-Offringa, I.A., 2000. Mol. Cell. Biol. 20, 4765–4772.

41. *Structural basis for recognition of AU-rich element RNA by the HuD protein.* Wang, X., Tanaka Hall, T.M., 2001. *Nat. Struct. Biol.* 8, 141–145.
42. *Novel recognition motifs and biological functions of the RNA-binding protein HuD revealed by genome-wide identification of its targets.* Bolognani, F., Contente-Cuomo, T., Perrone-Bizzozero, N.I., 2010. *Nucleic Acids Res.* 38, 117–130.
43. *Neuronal Elav-like (Hu) proteins regulate RNA splicing and abundance to control glutamate levels and neuronal excitability.* Ince-Dunn, G., Okano, H.J., Jensen, K.B., Park, W.Y., Zhong, R., Ule, J., Mele, A., Fak, J.J., Yang, C., Zhang, C., Yoo, J., Herre, M., Okano, H., Noebels, J.L., Darnell, R.B., 2012. *Neuron* 75, 1067–1080.
44. *Transcriptome-wide analysis of regulatory interactions of the RNA-binding protein HuR.* Lebedeva, S., Jens, M., Theil, K., Schwanhausser, B., Selbach, M., Landthaler, M., Rajewsky, N., 2011. *Mol. Cell* 43, 340–352.
45. *Integrative regulatory mapping indicates that the RNA-binding protein HuR couples pre-mRNA processing and mRNA stability.* Mukherjee, N., Corcoran, D.L., Nusbaum, J.D., Reid, D.W., Georgiev, S., Hafner, M., Ascano Jr., M., Tuschl, T., Ohler, U., Keene, J.D., 2011. *Mol. Cell* 43, 327–339.
46. *ARED 3.0: the large and diverse AU-rich transcriptome.* Bakheet, T., Williams, B.R., Khabar, K.S., 2006. *Nucleic Acids Res.* 34, D111–D114
47. *AU-rich elements: characterization and importance in mRNA degradation.* Chen, C.Y., Shyu, A.B., 1995. *Trends Biochem. Sci.* 20, 465–470.
48. *AU-rich elements and associated factors: are there unifying principles?* Barreau, C., Paillard, L., Osborne, H.B., 2006. *Nucleic Acids Res.* 33, 7138–7150.
49. *The RNA-binding protein HuD regulates neuronal cell identity and maturation.* Akamatsu, W., Fujihara, H., Mitsunashi, T., Yano, M., Shibata, S., Hayakawa, Y., Okano, H.J., Sakakibara, S., Takano, H., Takano, T., Takahashi, T., Noda, T., Okano, H., 2005. *Proc. Natl. Acad. Sci. U. S. A.* 102, 4625–4630.
50. *Overexpression of HuD accelerates neurite outgrowth and increases GAP-43 mRNA expression in cortical neurons and retinoic acid-induced embryonic stem cells in vitro.* Anderson, K.D., Sengupta, J., Morin, M., Neve, R.L., Valenzuela, C.F., Perrone-Bizzozero, N.I., 2001. *Exp. Neurol.* 168, 250–258.
51. *ELAV tumor antigen, Hel-N1, increases translation of neurofilament M mRNA and induces formation of neurites in human teratocarcinoma cells.* Antic, D., Lu, N., Keene, J.D., 1999. *Genes Dev.* 13, 449–461.
52. *Embryonic lethal abnormal vision-like RNA-binding proteins regulate neurite outgrowth and tau expression in PC12 cells.* Aranda-Abreu, G.E., Behar, L., Chung, S., Furneaux, H., Ginzburg, I., 1999. *J. Neurosci.* 19, 6907–6917.
53. *Expression of HuD protein is essential for initial phase of neuronal differentiation in rat pheochromocytoma PC12 cells.* Dobashi, Y., Shoji, M., Wakata, Y., Kameya, T., 1998. *Biochem. Biophys. Res. Commun.* 244, 226–229.

54. *The RNA-binding protein HuD is required for GAP-43 mRNA stability, GAP-43 gene expression, and PKC-dependent neurite outgrowth in PC12 cells.* Mobarak, C.D., Anderson, K.D., Morin, M., Beckel-Mitchener, A., Rogers, S.L., Furneaux, H., King, P., Perrone-Bizzozero, N.I., 2000. *Mol. Biol. Cell* 11, 3191–3203.
55. *Mammalian ELAV-like neuronal RNA-binding proteins HuB and HuC promote neuronal development in both the central and the peripheral nervous systems.* Akamatsu, W., Okano, H.J., Osumi, N., Inoue, T., Nakamura, S., Sakakibara, S., Miura, M., Matsuo, N., Darnell, R.B., Okano, H., 1999. *Proc. Natl. Acad. Sci. U. S. A.* 96, 9885–9890.
56. *EGF converts transit-amplifying neurogenic precursors in the adult brain into multipotent stem cells.* Doetsch F, Petreanu L, Caille I, Garcia-Verdugo JM, Alvarez-Buylla A. , 2002 *Dec 19;36(6):1021-34.*
57. *EGF mutant receptor vIII as a molecular target in cancer therapy.* Kuan CT, Wikstrand CJ, Bigner DD. *Endocrine-Related Cancer* 2001.
58. *Molecular biology of gliomas.* Lassman AB. *Current Neurology and Neuroscience Reports* 2004.
59. *The role of the subependymal plate in glial tumorigenesis.* Vick NA, Lin Mj, Bigner DD. *Acta Neuropathologica*, 1977.
60. *The origin of experimental brain tumors: a sequential study.* Lantos PL, Cox DJ. *Experientia* 1976.
61. *Relationship of glioblastoma multiforme to neural stem cell regions predicts invasive and multifocal tumor phenotype.* Lim DA, Cha S, Mayo MC, et al, *Neuro Oncol* 2007;9:424-429.
62. *The role of elav-like genes, a conserved family encoding RNA-binding proteins, in growth and development.* Good, P. J. (1997) *Semin. Cell Dev. Biol.* 8, 577 – 584,
63. *RNA-binding proteins and neural development: a matter of targets and complexes.* Agnes, F. and Perron, M. (2004) *Neuroreport* 15, 2567 – 2570
64. *Hel-N1/Hel-N2 proteins are bound to poly(A)<sup>+</sup> mRNA in granular RNP structures and are implicated in neuronal differentiation.* Gao, F. B. and Keene, J. D. (1996) *J. Cell Sci.* 109 (Pt 3), 579 – 589
65. *HuR and mRNA stability.* Brennan, C. M. and Steitz, J. A. (2001) *Cell Mol. Life Sci.* 58, 266 – 277
66. *Poly(A) tail length-dependent stabilization of GAP-43 mRNA by the RNA-binding protein HuD.* Beckel-Mitchener, AC. 2002,
67. *HNS, a nuclear cytoplasmic shuttling sequence in HuR.* Fan X.C. and Steitz J.A: (1998).
68. *RNA-binding protein HuR enhances p53 translation in response to ultraviolet light irradiation;* Krystyna Mazan-Mamczarz,\* Stefanie Galbán,\* Isabel López de

Silanes,\* Jennifer L. Martindale,\* Ulus Atasoy,† Jack D. Keene,† and Myriam Gorospe (2003)

69. *Translational control of cytochrome c by RNA binding proteins TIA-1 and HuR* Mol Cell Biol. 2006 Apr; Kawai T, Lal A, Yang X, Galban S, Mazan-Mamczarz K, Gorospe M. (2006);
70. *Ectopic expression of Hel-N1, an RNA binding protein, increases glucose transporter (GLUT1)* ; Feb; Jain RG, Andrews LG, McGowan KM, Pekala PH, Keene JD. Mol Cell Biol. 1997
71. *ELAV/hu proteins inhibit p27 translation via an IRES element in the p27 5'UTR*. Kullmann M, Göpfert U, Siewe B, Hengst L. Genes Dev. 2002 Dec 1;
72. *A conserved family of elavl-like genes in vertebrates*; Good PJ. Proc Natl Acad Sci U S A. 1995 May 9;
73. *Expression of mRNA for the elavl-like neuronal specific RNA binding protein, HuD during nervous system development*. Clayton GH, Perez GM, Smith RL, Owens GC. Brain Res Dev Brain Res. 1998 Aug 8;
74. *Emerging complexity of the HuD/ELAVL4 gene; implications for neuronal development, function, and dysfunction*. Lucas M, Bronicki And Bernard J. Jasmin.. RNA 19:1019–1037
75. *Cytoplasmic expression of the ELAV-like protein HuR as a potential prognostic marker in esophageal squamous cell carcinoma*. Zhang C, Xue G, Bi J, Geng M, Chu H, Guan Y, Wang J, Wang B. Tumour Biol. 2013 Jul 20
76. *miR-29 Acts as a Decoy in Sarcomas to Protect the Tumor Suppressor A20 mRNA from Degradation by HuR*. Yaseen Balkhi M, Iwenofu OH, Bakkar N, Ladner KJ, Chandler DS, Houghton PJ, London CA, Kraybill W, Perrotti D, Croce CM, Keller C, Guttridge DC. Sci Signal. 2013 Jul 30
77. *Trichostatin-A Modulates Claudin-1 mRNA Stability through the Modulation of Hu antigen R and Tristetraprolin in Colon Cancer Cells*. Sharma A, Bhat AA, Krishnan M, Singh AB, Dhawan P . Carcinogenesis. 2013 Jul 23.
78. *Cytoplasmic HuR expression correlates with cIAP2 expression and clinicopathologic factors in oral squamous cell carcinoma cells*. Cha JD, Kim HK, Cha IH. Head Neck. 2013 Jul 15.
79. *HuR is a post-transcriptional regulator of core metabolic enzymes in pancreatic cancer*. Burkhart RA, Pineda DM, Chand SN, Romeo C, Londin ER, Karoly ED, Cozzitorto JA, Rigoutsos I, Yeo CJ, Brody JR, Winter JM. RNA Biol. 2013 Jun 13;
80. *Methionine Adenosyltransferase 2B, HuR and Sirtuin 1 Crosstalk Impacts on Resveratrol's Effect on Apoptosis and Growth in Liver Cancer Cells*. Yang H, Zheng Y, Li TW, Peng H, Fernandez Ramos D, Martínez-Chantar ML, Rojas AL, Mato JM, Lu SC. J Biol Chem. 2013 Jun 28.



81. *Anti-HuC and -HuD autoantibodies are differential sero-diagnostic markers for small cell carcinoma from large cell neuroendocrine carcinoma of the lung.* Matsumoto T, Ryuge S, Kobayashi M, Kageyama T, Hattori M, Goshima N, Jiang SX, Saegusa M, Iyoda A, Satoh Y, Masuda N, Sato Y . *Int J Oncol.* 2012 Jun.
82. *Molecular analysis of the HuD gene in neuroendocrine lung cancers.* D'Alessandro V, Muscarella LA, la Torre A, Bisceglia M, Parrella P, Scaramuzzi G, Storlazzi CT, Trombetta D, Kok K, De Cata A, Sperandio M, Zelante L, Carella M, Vendemiale G. *Lung Cancer.* 2010 Jan.
83. *Cancerous stem cells can arise from pediatric brain tumors.* Hemmati HD, Nakano I, Lazareff JA, Masterman-Smith M, Geschwind DH, Bronner-Fraser M, Kornblum HI. *Proc Natl Acad Sci U S A.* 2003 Dec 9.
84. *Adult Neural Stem Cells .* Rossella Galli , Angela Gritti, Angelo L. Vescovi. *Methods Mol Biol.* 2008
85. *Allelic losses at 1p36 and 19q13 in gliomas: correlation with histologic classification, definition of a 150-kb minimal deleted region on 1p36, and evaluation of CAMTA1 as a candidate tumor suppressor gene.* Barbashina V, Salazar P, Holland EC, et al. *Clin Cancer Res.*2005;11:1119–28.
86. *Role of the p16 tumor suppressor gene in cancer.* Liggett WH Jr, Sidransky D. *J Clin Oncol.* 1998 Mar;16(3):1197-206.
87. *In vitro scratch assay: a convenient and inexpensive method for analysis of cell migration in vitro.* Liang CC, Park AY, Guan JL; *Nat Protoc.* 2007
88. *Widespread uncoupling between transcriptome and translatome variations after a stimulus in mammalian cells.* Tebaldi T, Re A, Viero G, Pegoretti I, Passerini A, Blanzieri E, Quattrone A. *BMC Genomics.* 2012 Jun 6;13:220. doi: 10.1186/1471-2164-13-220.
89. *SOX2 silencing in glioblastoma tumor-initiating cells causes stop of proliferation and loss of tumorigenicity.* Gangemi RM, et al, *Stem Cells.* 2009 Jan;27(1):40-8.
90. *The Sox2 response program in glioblastoma multiforme: an integrated ChIP-seq, expression microarray, and microRNA analysis.* Fang X, Yoon JG, Li L, Yu W, Shao J, Hua D, Zheng S, Hood L, Goodlett DR, Foltz G, Lin B. *BMC Genomics.* 2011 Jan 6;
91. *Nestin: Neural Stem/Progenitor Cell Marker in Brain Tumors,* By Yoko Matsuda, Hisashi Yoshimura, Taeko Suzuki and Toshiyuki Ishiwata. Chapter 23, "Evolution of the Molecular Biology of Brain Tumors and the Therapeutic Implications"
92. *Neuroepithelial stem cell marker nestin regulates the migration, invasion and growth of human gliomas.* Ishiwata T, Teduka K, Yamamoto T, Kawahara K, Matsuda Y, Naito Z. *Oncol Rep.* 2011 Jul;
93. *Diagnostic utility of neural stem and progenitor cell markers nestin and SOX2 in distinguishing nodal melanocytic nevi from metastatic melanomas.* Chen PL, Chen WS, Li J, Lind AC, Lu D.

94. *Neurosphere formation is an independent predictor of clinical outcome in malignant glioma.* Dan R. Laks, Michael Masterman-Smith, Koppany Visnyei, Brigitte Angenieux, Nicholas M. Orozco, Ian Foran, William H. Yong, Harry V. Vinters, Linda M. Liao, Jorge A. Lazareff, Paul S. Mischel, Timothy F. Cloughesy, Steve Horvath, and Harley I. Kornblum. *Stem Cells*. 2009 April; 27(4): 980–987.
95. *TCGA-Consortium. 2008. Comprehensive genomic characterization defines human glioblastoma genes and core pathways.* *Nature*, 455:1061–1068.
96. *InterPro in 2011: new developments in the family and domain prediction database* Hunter S, Jones P, Mitchell A, Apweiler R, Attwood TK, Bateman A, Bernard T et al. (2011). *Nucleic Acids Research*, doi: 10.1093/nar/gkr948.
97. *Insights into RNA Biology from an Atlas of Mammalian mRNA-Binding Proteins* Castello, A., Fischer, B., Eichelbaum, K., Horos, R., Beckmann, B. M., Strein, C., Davey, N. E., et al. (2012).. *Cell*, 149(6):1393–1406.
98. *Integrated genomic analysis identifies clinically relevant subtypes of glioblastoma characterized by abnormalities in PDGFRA, IDH1, EGFR, and NF1.* Verhaak RG, Hoadley KA, Purdom E, Wang V, Qi Y, Wilkerson MD, Miller CR et al. (2010) *Cancer Cell*, 17(1):98-110.
99. National Cancer Institute. 2005. REMBRANDT home page. <http://rembrandt.nci.nih.gov>. Accessed 2013 January 24.
100. *AURA: Atlas of UTR Regulatory Activity* .Dassi E, Malossini A, Re A, Tebaldi T, Mazza T, Caputi L, Quattrone A. (2011). *Bioinformatics*, doi: 10.1093/bioinformatics/btr608.
101. Gartel AL, Radhakrishnan SK., *Cancer Res*. 2005 May, Lost in transcription: p21 repression, mechanisms, and consequences.
102. *Glioma stem cells: a midterm exam.* Stiles CD, Rowitch DH., *Neuron*. 2008 Jun 26
103. *Hel-N1: an autoimmune RNA-binding protein with specificity for 3' uridylate-rich untranslated regions of growth factor mRNAs.* Mol Cell Biol. 1993 June; 13 T D Levine, F Gao, P H King, L G Andrews, and J D Keene.
104. *Hel-N1, an RNA-binding protein, is a ligand for an A + U rich region of the GLUT1 3'UTR.* Jain, R. G., Andrews, L. G., McGowan, K. M., Gao, F., Keene, J. D. and Pekala, P. P. (1995) *Nucleic Acids Symp Ser*. 33, 209 – 211
105. *Mammalian homologs of Drosophila ELAV localized to a neuronal subset can bind in vitro to the 3' UTR of mRNA encoding the Id transcriptional repressor.* King, P. H., Levine, T. D., Freneau, R. T. Jr and Keene, J.D.(1994) *J Neurosci*. 14,1943 – 1952.
106. *RNA-binding analyses of HuC and HuD with the VEGF and c-myc 3'-untranslated regions using a novel ELISA-based assay.* King, P. H. (2000) *Nucleic Acids Res*. 28, E20.
107. *HuD, a neuronal-specific RNA-binding protein, is a potential regulator of MYCN expression in human neuroblastoma cells* Ross, R. A, Lazarova, D. L., Manley, G. T.,

- Smitt, P. S., Spengler, B. A., Posner, J. B. and Biedler, J. L. (1997). *Eur J Cancer*. 33, 2071 – 2074.
108. *p21(waf1) mRNA contains a conserved element in its 3'-untranslated region that is bound by the Elav-like mRNA-stabilizing proteins.* Joseph, B., Orlian, M. and Furneaux, H. (1998) *J Biol Chem*. 273, 20511 – 20516.
109. *Post-transcriptional regulation of acetylcholinesterase mRNAs in nerve growth factor-treated PC12 cells by the RNA-binding protein HuD* Deschenes-Furry, J., Belanger, G., Perrone-Bizzozero, N. and Jasmin, B. J. (2003). *J Biol Chem*. 278, 5710 – 5717
110. *The Elav-like proteins bind to a conserved regulatory element in the 3'-untranslated region of GAP-43 mRNA.* Chung, S., Eckrich, M., Perrone-Bizzozero, N., Kohn, D. T. and Furneaux, H. (1997) *J Biol Chem*. 272, 6593 – 6598
111. *HuD binds to three AU-rich sequences in the 3'-UTR of neuroserpin mRNA and promotes the accumulation of neuroserpin mRNA and protein.* Cuadrado, A., Navarro-Yubero, C., Furneaux, H., Kinter, J., Sonderegger, P. and Muçoz, A. (2002) *Nucleic Acids Res*. 30, 2202 – 2211.
112. *A role for the ELAV RNA-binding proteins in neural stem cells: stabilization of Msi1 mRNA.* Ratti, A., Fallini, C., Cova, L., Fantozzi, R., Calzarossa, C., Zennaro, E., Pascale, A., Quattrone, A. and Silani, V. (2006) *J. Cell Sci*. 119, 1442 – 1452
113. *The 3'-UTR of the mRNA coding for the major protein kinase C substrate MARCKS contains a novel CU-rich element interacting with the mRNA stabilizing factors HuD and HuR.* Wein, G., Rçssler, M., Klug, R. and Herget, T. (2003) *Eur J Biochem*. 270, 350 – 365.
114. *A nuclear function of Hu proteins as neuron-specific alternative RNA processing regulators.* Zhu, H., Hasman, R. A., Barron, V. A., Luo, G. and Lou, H. (2006) *Mol. Biol. Cell* 17, 5105 – 5114
115. *Localization of human elav-like neuronal protein 1 (Hel-N1) on chromosome 9p21 by chromosome microdissection polymerase chain reaction and fluorescence in situ hybridization.* Han, J., Knops, J. F., Longshore, J. W., King, P. H. *Genomics* 36: 189-191, 1996
116. *Relationship between p21 expression and mutation of the p53 tumor suppressor gene in normal and malignant ovarian epithelial cells.* Clin Cancer Res. 1996 Sep; Elbendary AA, Cirisano FD, Evans AC Jr, Davis PL, Iglehart JD, Marks JR, Berchuck A.
117. *shRNA knockdown of Bmi-1 reveals a critical role for p21-Rb pathway in NSC self-renewal during development.* Cell Stem Cell. 2007 Jun 7;1(1):87-99. Fasano CA, Dimos JT, Ivanova NB, Lowry N, Lemischka IR, Temple S.

118. *Posttranscriptional regulation of cancer traits by HuR*. Abdelmohsen K, Gorospe M. Wiley Interdiscip Rev RNA. 2010 Sep-Oct;1(2):214-29. doi: 10.1002/wrna.4. Epub 2010 May 6. Review. PMID: 21935886
119. *mRNA stability alterations mediated by HuR are necessary to sustain the fast growth of glioma cells*. Bolognani F, Gallani AI, Sokol L, Baskin DS, Meisner-Kober N. J Neurooncol. 2012 Feb;106(3):531-42. doi: 10.1007/s11060-011-0707-1. Epub 2011 Sep 21. PMID:21935689
120. *HuR, a RNA stability factor, is expressed in malignant brain tumors and binds to adenine- and uridine-rich elements within the 3' untranslated regions of cytokine and angiogenic factor mRNAs*. Nabors LB, Gillespie GY, Harkins L, King PH. Cancer Res. 2001 Mar 1;61(5):2154-61. PMID: 11280780,
121. *The RNA-binding protein HuR promotes glioma growth and treatment resistance*. Filippova N, Yang X, Wang Y, Gillespie GY, Langford C, King PH, Wheeler C, Nabors LB. Mol Cancer Res. 2011 May;9(5):648-59. doi: 10.1158/1541-7786.MCR-10-0325. Epub 2011 Apr 15. PMID: 21498545
122. *Neuron-specific ELAV/Hu proteins suppress HuR mRNA during neuronal differentiation by alternative polyadenylation*. Mansfield KD, Keene JD. Nucleic Acids Res. 2012 Mar;40(6):2734-46. doi: 10.1093/nar/gkr1114. Epub 2011 Dec 1. PMID: 22139917
123. *p21(waf1) mRNA contains a conserved element in its 3'-untranslated region that is bound by the Elav-like mRNA-stabilizing proteins*. Joseph B, Orlian M, Furneaux H. J Biol Chem. 1998 Aug 7;273(32):20511-6. PMID: 9685407
124. *The 3'-untranslated region of p21WAF1 mRNA is a composite cis-acting sequence bound by RNA-binding proteins from breast cancer cells, including HuR and poly(C)-binding protein*. Giles KM, Daly JM, Beveridge DJ, Thomson AM, Voon DC, Furneaux HM, Jazayeri JA, Leedman PJ. J Biol Chem. 2003 Jan 31;278(5):2937-46. Epub 2002 Nov 12. PMID:12431987
125. *p21 loss compromises the relative quiescence of forebrain stem cell proliferation leading to exhaustion of their proliferation capacity*. Kippin, T.E., Martens, D.J., and van der Kooy, D. (2005). Genes Dev 19, 756-767.

126. *Rank products: a simple, yet powerful, new method to detect differentially regulated genes in replicated microarray experiments.* FEBS Lett. 2004 Aug 27; Breitling R, Armengaud P, Amtmann A, Herzyk P.

## **8. APPENDIX**

### **Copy number alterations (CNAs) can be detected by qPCR using SYBR-GREEN**

To validate the capacity of SYBR-GREEN qPCR method in discriminating copy number alterations (CNA), an analysis on MECP2, a gene present on chromosome X, was performed on genomic DNA of males and females. SNRPF and CTDSP1 were used as reference genes. The internal control used for this analysis was a female sample. As it can be shown in *Figure A.1* the analysis worked perfectly: the amount of MECP2 gene is twice in female sample compared to male samples. The SYBR-GREEN qPCR method worked and was used to evaluate CNAs.

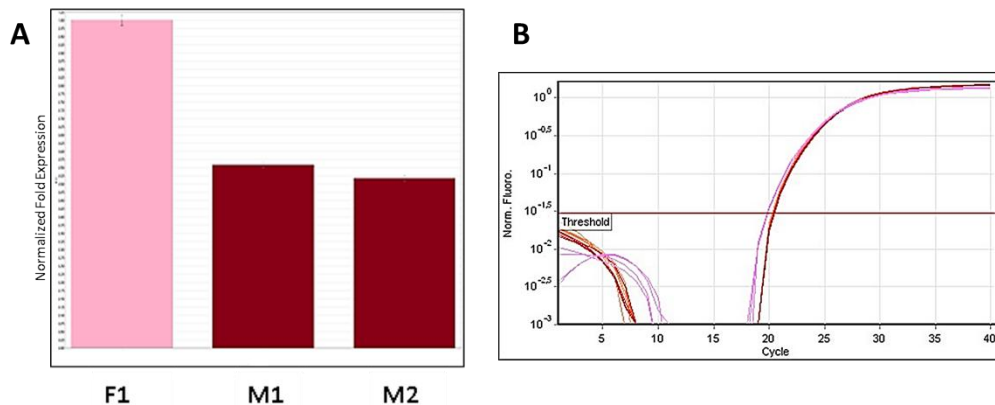


**Figure A.1: Evaluation of copy number of MECP2 in males and females DNA samples using qPCR. (A)** F1 (pink bar) is a female, M1 and M2 (red bars) are males. Pink bar is twice of red bars meaning that MECP2 is present in two copies. **(B)** Pink expression curve is a female sample, whereas the red expression curves are male samples. Pink curve is earlier than red curves, meaning that the amount of DNA is higher.

As the data show, the level of MECP2 in the female is twice the level in males (see *Figure A.1.A*), meaning that MECP2 gene is present in two copies in female samples compare the male samples. Observing the qPCR curves (*Figure A.1.B*), the pink curve (female curve) is first to the red curves (male curves) meaning that the amount of DNA is higher in female sample compare the male samples.

This analysis confirmed that qPCR, performed with SYBR-GREEN and gene specific primers, can detect copy number alterations. Each range of the *Table 9* was set fitting a median value and, from that point, minimum closed extremities were set to maximize the evaluation, improving the accuracy. For each samples, the value corresponding to Unfold Expression on CFX Manager™ Software 184-5000 (Version 3.0, Bio-Rad) was compared to this scale (*Table A.1*) to detect CNAs.

**Table A.1: Scale used to evaluate copy number variations.** The value relative to unscaled expression value are compared with this scale to determine the allele's number.

COPY NUMBER	RANGE	RESULT
0	-0,24 – 0 – 0,24	HOMOZYGOUS DELETION
1	0,25 – 0,5 – 0,75	HETEROZYGOUS DELETION
2	0,76 – 1 – 1,25	NORMAL
3	1,26 – 2 – 1,75	3 COPIES
4	1,76 – 2,5 – 2,25	4 COPIES

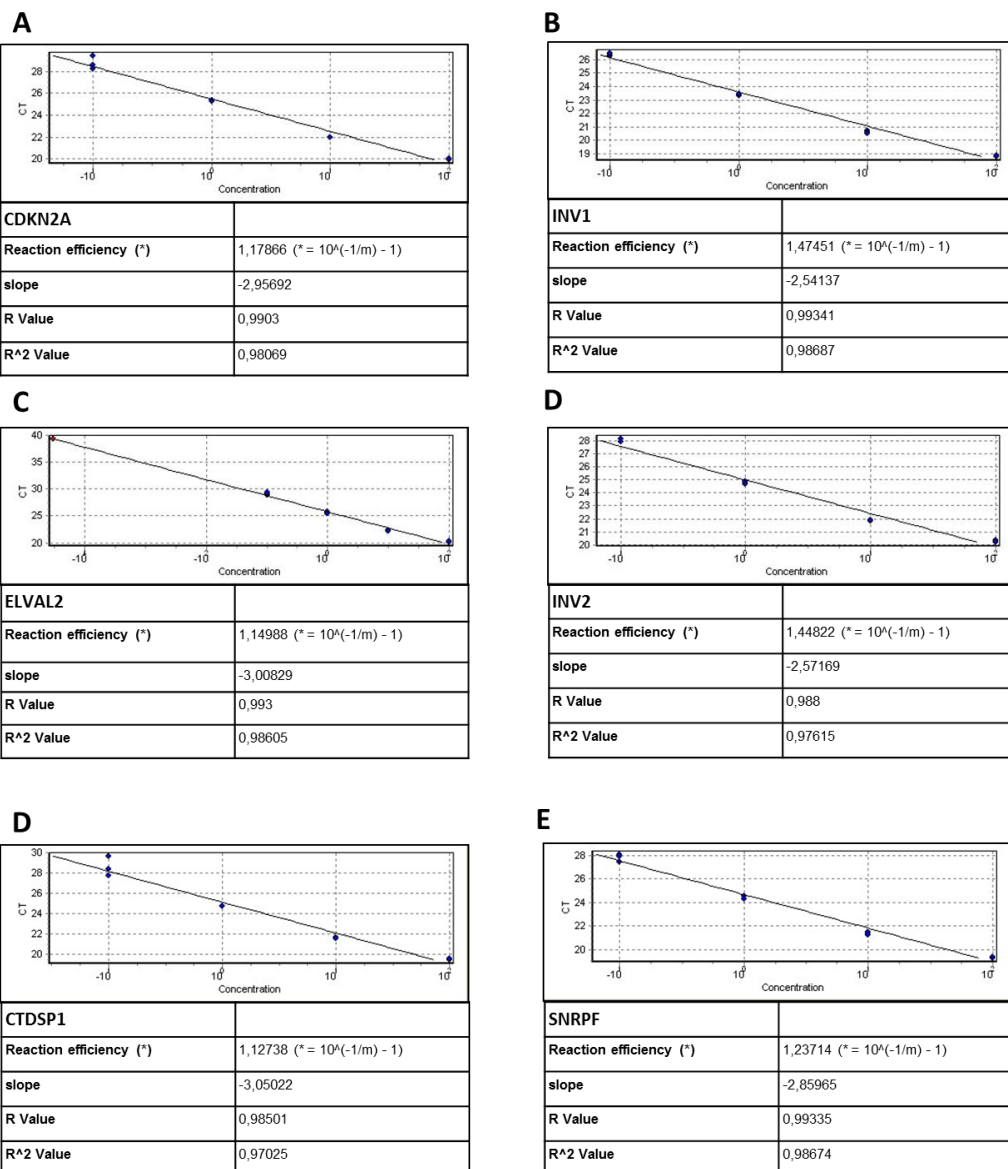


**Figure A2:** From A to E panels are reported the standard curve for each couple of primers and the relative values of efficiencies (estimated from the slope (m) :  $E = 10^{(-1/m) - 1}$ ), which are almost identical and therefore amplifying at the same rate, meaning an accurate quantification of CNV.